EPHOU-14-006

Probing Neutrino in Muon Decay at Finite Distance

Kenzo Ishikawa, Tasuku Nozaki, Masashi Sentoku, and Yutaka Tobita

Department of Physics, Faculty of Science,

Hokkaido University, Sapporo 060-0810, Japan

(Dated: October 20, 2014)

arXiv:1405.0582v2 [hep-ph] 17 Oct 2014

Abstract

New physical observables of the neutrino from muon decay derived from the spectrum in non-asymptotic region of $T \leq \tau_\mu$ are presented. The probability of the events that the neutrino is detected is the sum $T\Gamma^0 + P^{(d)}$, where each of them reveals the particle and wave characteristics. Γ^0 is computed with Fermi's golden rule, whereas $P^{(d)}$ is new and is computed with a new method. $P^{(d)}$ has unusual properties caused by the overlap of the initial and final wave functions, and becomes significant for neutrinos. Neutrino mixing affects $P^{(d)}$ and Γ^0 differently, and the probability of the event that the particular neutrino is detected, in the distance $L \leq L_0$, and $L \leq c\tau_\mu$, where $L_0 = m_\nu^2/(2E_\nu)$ and τ_μ is the life-time of muon, becomes sensitive to the absolute neutrino masses and mixing angles. Including $P^{(d)}$ of three neutrinos, all neutrino experiments made to confirm LSND data become consistent each other, and the future precision experiments will be able to determine the absolute neutrino masses.

I. INTRODUCTION

The muon decay has been studied in the space time region where the waves of initial and final states separate and behave like particles, which we call particle-zone, and been in accord with the experiments satisfying this condition [1]. If the waves overlap, which we call wave-zone, they do not behave like particles and cause interference of the quantum mechanical waves. The transition probability is modified from that of the particle-zone, but full analysis has been left uncompleted [2]. Precision experiments on the muon decay including this region are under way, and the theoretical analysis in the wave-zone is necessary.

The amplitude in the asymptotic region obtained with the Feynman diagram corresponds to that of the particle-zone by $i\epsilon$ prescription, where a wave in the asymptotic region is expressed with a line and behaves like a particle. In the wave-zone, the amplitude reveals characteristics of quantum waves. The previous papers developed the theory for the wave-zone [3, 4] and is applied to the muon three-body decays. The state vector satisfies the many-body Schrödinger equation which is linear, and the solution satisfies the superposition principle. Consequently, the quantum mechanical diffraction caused by many-body interactions arises without disorder. It was found that the probability of the event that the decay products are detected is composed of two components at $T \leq \tau_\pi$ such that the probability has dual natures of the particle and wave, where T is time interval between in and out states and τ_π is the average life time of the pion,

$$P = T\Gamma^0 + P^{(d)}. \tag{1}$$

Owing to the particle or wave characteristics, Γ^0 preserves the symmetries of the free Lagrangian, and $P^{(d)}$ breaks some of them.

$P^{(d)}$ is extremely small in the atomic transitions and others [3] and has been considered negligible, and paid no attention until recently. However that is not the case in various phenomena and experiments in wide area such as radiative transitions or weak decays involving neutrinos of local or nearly local objects. Large $P^{(d)}$ appears as unavoidable consequences of quantum mechanics, and manifests the wave natures revealing unusual properties such as the non-conservation of kinetic energy, the violation of some selection rules, and the large mass dependence. For the process of large $P^{(d)}$, the energy spectrum deviates, and $P^{(d)}$ is necessary for the comparison of the experiments with the theory and for a deep understanding of the natural phenomena. In the pion decay, $P^{(d)}$ is large for the neutrinos, and new

physical quantities derived from it are in accord with experiments and useful to determine the absolute neutrino mass.

Now we consider the muon decay. The electron spectra in muon decays

$$\mu^- \to e^- + \bar{\nu}_e + \nu_\mu, \tag{2}$$

$$\mu^+ \to e^+ + \nu_e + \bar{\nu}_\mu, \tag{3}$$

agree with the theory without $P^{(d)}$, which indicates that $P^{(d)}$ is unnecessary for the electron, but may not so for the neutrinos due to the large mass difference between the electron and neutrino. The previous neutrino experiments actually have shown inconsistency among those of different geometries, if $P^{(d)}$ is ignored. Accordingly it is urgent to find if the probability for the neutrino follows also Eq. (1), having large corrections to the standard formula, which is the subject of the present paper. First we examine if the wave function at finite t derived from the Schrödinger equation

$$\begin{aligned} i\hbar\frac{\partial}{\partial t}|\Psi(t)\rangle &= H|\Psi(t)\rangle = (H_0 + H_{\rm int})\,|\Psi(t)\rangle, \\ H_0 &= \int d\vec{x} \sum_{l=e,\mu} \left(\bar{l}(x)\left(\vec{\alpha}\cdot\vec{\nabla} + \beta m_l\right) l(x) + \bar{\nu}_l(x)\left(\vec{\alpha}\cdot\vec{\nabla} + \beta m_{\nu_l}\right)\nu_l(x)\right), \\ H_{\rm int} &= \frac{G_F}{\sqrt{2}}\int d\vec{x}\,(\bar{\mu}(x)\,(1-\gamma_5)\,\gamma_\mu\nu_\mu(x))\,(\bar{e}(x)\,(1-\gamma_5)\,\gamma^\mu\nu_e(x))^\dagger\,, \end{aligned} \tag{4}$$

where G_F is the Fermi coupling constant for the case of no-mixing, which is linear in $|\Psi(t)\rangle$ shows $P^{(d)}$. The $H_{\rm int}$ causes non-linear interaction among the Dirac fields, and causes $|\Psi(t)\rangle$ to be expressed by a superposition of many-body states. For one muon state of the momentum $\vec{p}_\mu$ at $t=0$, that is

$$|\Psi(t),\vec{p}\rangle = a_0(t)|\vec{p}_\mu\rangle + \int d\vec{p}_e d\vec{p}_{\nu_e} d\vec{p}_{\nu_\mu} a_1(t,\vec{p}_e,\vec{p}_{\nu_e},\vec{p}_{\nu_\mu})|\vec{p}_e,\vec{p}_{\nu_e},\vec{p}_{\nu_\mu}\rangle, \tag{5}$$

$$a_0(t) = e^{-i\frac{E_\mu}{\hbar}t-\frac{t}{\tau_\mu}},\ a_1(t,\vec{p}_e,\vec{p}_{\nu_e},\vec{p}_{\nu_\mu}) = e^{-i\frac{E_\mu}{\hbar}t}\frac{e^{-i\frac{\omega}{\hbar}t} - e^{-\frac{t}{\tau_\mu}}}{\omega + i\frac{\hbar}{\tau_\mu}}\langle\vec{p}_e,\vec{p}_{\nu_e},\vec{p}_{\nu_\mu}|H_{\rm int}|\vec{p}_\mu\rangle, \tag{6}$$

in the lowest order of G_F, where $\omega = E_e + E_{\nu_e} + E_{\nu_\mu} - E_\mu$ and τ_μ is the muon's life time. The state satisfies

$$\frac{\langle\Psi(t)|H_{\rm int}|\Psi(t)\rangle}{\langle\Psi(t)|\Psi(t)\rangle} = 2\int d\vec{p}_e d\vec{p}_{\nu_e} d\vec{p}_{\nu_\mu}\zeta(\omega,t,\tau_\mu)\left|\langle\vec{p}_e,\vec{p}_{\nu_e},\vec{p}_{\nu_\mu}|H_{\rm int}|\vec{p}_\mu\rangle\right|^2, \tag{7}$$

$$\zeta(\omega,t,\tau_\mu) = e^{-\frac{t}{\tau_\mu}}\frac{\omega\cos(\omega t/\hbar) - \omega e^{-\frac{t}{\tau_\mu}} - \frac{\hbar}{\tau_\mu}\sin(\omega t/\hbar)}{\omega^2 + \frac{\hbar^2}{\tau_\mu^2}}, \tag{8}$$

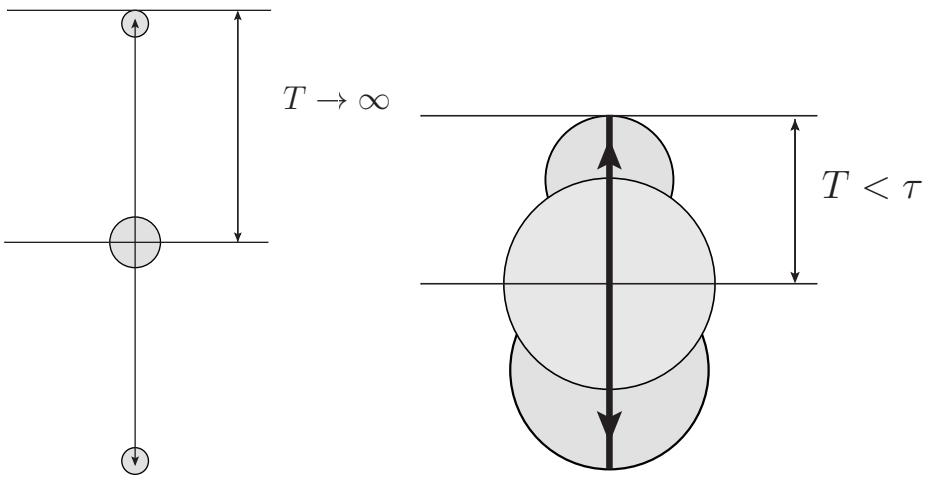

FIG. 1. Two-body decays of a particle of life time τ at $T \to \infty$ (left) and $T < \tau$ (right). At $T \to \infty$ the initial state does not overlap with the final state but at $T < \tau$, the initial state overlaps with the final state. Because of this overlapping region, kinetic energy does not conserve at $T < \tau$.

and

$$\delta E(t) = \langle \Psi(t)|(i\hbar\frac{\partial}{\partial t} - E_\mu)|\Psi(t)\rangle = \langle \Psi(t)|H_{\rm int}|\Psi(t)\rangle \begin{cases} = 0;\ t = 0,\ \infty, \\ \neq 0;\ 0 < t < \tau_\mu. \end{cases} \tag{9}$$

The expectation value of $(i\hbar\frac{\partial}{\partial t} - E_\mu)$ does not vanish, and the kinetic energy defined by the Einstein's relation from frequency does not hold the exact conservation law. $\delta E(t)$ is extremely small in magnitude, but the ratio between $\delta E(t)$ and the norm of the state

$$\frac{\delta E(t)}{\langle \Psi_{e,\nu_e,\nu_\mu}(t)|\Psi_{e,\nu_e,\nu_\mu}(t)\rangle} = O(1), \tag{10}$$

is order unity, where $\Psi_{e,\nu_e,\nu_\mu}(t)$ is the state that has the electron and neutrinos. Thus the waves overlap and cause $P^{(d)}$ to be non-negligible.

The $P^{(d)}$ can be estimated from the waves of satisfying $\omega \neq 0$ included in $|\Psi(t), \vec{p}\rangle$. Especially those states of infinitely large p_e or p_ν included from Eq. (6) give effects peculiar to relativistic waves. Suppose these states couple with a field $\psi(x)$, then a correlation function $\Delta(x-y) = \langle \Psi|\psi^\dagger(x)\psi(y)|\Psi\rangle$ becomes a superposition of relativistic waves $\int d\vec{q} e^{i(E(\vec{q})(x-y)^0 - \vec{q}\cdot(\vec{x}-\vec{y}))/\hbar}$, which includes $\delta((x-y)^2)$. A combination of this singularity with another wave of the energy and momentum $(E(\vec{p}), \vec{p})$, which will be shown to constitute a main part of $P^{(d)}$ later, is

$$e^{i(E(\vec{p})(x-y)^0 - \vec{p}\cdot(\vec{x}-\vec{y}))/\hbar}\delta((x-y)^2) = e^{i(E(\vec{p}) - |\vec{p}|\cos\theta)(x-y)^0/\hbar}\delta((x-y)^2), \tag{11}$$

where θ is the angle between $\vec{p}$ and $\vec{x}-\vec{y}$. At $\theta=0$ and $E(\vec{p})=\sqrt{\vec{p}^2c^2+m^2c^4}$, Eq. (11) becomes

$$e^{i\frac{m^2c^4}{2E\hbar}(x-y)^0}\delta((x-y)^2). \tag{12}$$

Thus the product shows the oscillation characterized by the angular velocity $\frac{m^2c^4}{2E\hbar}$, which accumulates the waves of the region $l \leq L_c$,

$$L_c = \frac{\hbar}{mc} \times \frac{E}{mc^2}, \tag{13}$$

where c, E, and m are the speed of light, the energy and mass of detected particle, respectively [3]. L_c is extremely large for the neutrino. Moreover, as is seen in Fig. 1, the overlapping region is proportional to the spatial size of wave denoted as σ. $P^{(d)}$ materializes these effects in the form

$$P^{(d)} = \sigma\frac{\hbar E}{m^2c^3} \times (\text{numerical factor}). \tag{14}$$

The neutrino flavor mixing in the wave-zone would give different effects from that in the particle-zone which agrees with the standard flavor oscillation, and give the probability sensitive to the absolute neutrino mass and mixing angles.

To compute $P^{(d)}$ rigorously, $S[T]$ of satisfying the boundary conditions at T defined before is used. The standard S-matrix, $S[\infty]$, satisfies those of asymptotic region $T\to\infty$ [2], hence is useless. $S[T]$ is unitary and formulated with Møller operator [4, 5]. For satisfying the boundary condition at T correctly, wave packets that are localized in space are used. $S[T]$ gives identical results as $S[\infty]$ in large T, and includes the correction in small T [3]. Boundary conditions of $S[T]$, for the scalar field $\phi(x)$, is [12]

$$\begin{aligned}\lim_{t\to-\mathrm{T}/2}\langle\alpha|\phi^f|\beta\rangle &= \langle\alpha|\phi^f_{in}|\beta\rangle \\ \lim_{t\to+\mathrm{T}/2}\langle\phi^f|0\rangle &= \langle\alpha|\phi^f_{out}|\beta\rangle,\end{aligned} \tag{15}$$

where $\phi_{\mathrm{in}}(x)$ and $\phi_{\mathrm{out}}(x)$ satisfy the free wave equation, and ϕ^f, ϕ^f_{in} and ϕ^f_{out} are the expansion coefficient of $\phi(x)$, $\phi_{\mathrm{in}}(x)$ and $\phi_{\mathrm{out}}(x)$, with the normalized wave functions $f(x)$ of the form

$$\phi^f(t) = i\int d^3x f^*(\vec{x},t)\overleftrightarrow{\partial_0}\phi(\vec{x},t). \tag{16}$$

It is noted that normalizable functions are localized in space and specified by their centers [5, 11].

Mass squared differences of neutrinos found from flavor oscillations [6] are $(7.53 \pm 0.18) \times 10^{-5}$ eV$^2/c^4$, and $(2.44 \pm 0.06) \times 10^{-3}$ eV$^2/c^4$ (normal hierarchy) or $(2.52 \pm 0.07) \times 10^{-3}$ eV$^2/c^4$ (inverted). Tritium beta decay has been used for determining the absolute value but the existing upper bound for the effective-electron-neutrino mass squared is of the order of 2 eV$^2/c^4$ [7]. From cosmology, the bounds for a sum of masses are 0.44 eV$/c^2$ [8, 9] and 0.23 eV$/c^2$ [10].

We analyze the muon decays in details and present the transition probabilities including the diffraction term and the mixing effects. It will be shown that they are sensitive to the absolute masses and mixing angles, and resolve the controversy on the previous experiments.

The present paper is organized in the following manner. In Sec. 2, the boundary conditions of the muon decay process are given. In Sec. 3, the electron neutrino is studied and its implications to the neutrino experiments are presented in Sec. 4. Summary is given in Sec. 5.

II. BOUNDARY CONDITIONS FOR MUON DECAYS

For the event specified by the initial and final states, the probability amplitude is computed with $S[T]$ which implements them through the boundary conditions. Thus the amplitude depends on $f(x)$ of Eq. (16), which for out-going states shows the wave function that the out-going wave interacts in a successive reaction in detector, if a measurement is made, or in a reaction in nature [11].

In neutrino experiments, the neutrino is identified by nucleus or atom in detector, and their wave functions are used for $f(x)$. Nuclei have sizes of the order of 10^{-15} m and the electrons bounded in atom have sizes of the order of 10^{-10} m. Density is constant inside the nucleus and decreases smoothly toward the edge and that of electron is almost the same. So Gaussian wave packets are good approximation and are used. In the previous work, it was found that the corrections to the approximation are almost negligible [4], and that the $P^{(d)}$ is independent of the shape of the wave packet and is universal. The Gaussian wave packets are applied throughout this paper. The neutrino and anti-neutrino interact with matter differently [13]. For ν_e that is detected by $^{12}C + \nu_e \to {}^{12}N_{g.s.} + e^-$ process, the target

nucleus ^{12}C of the size $12^{\frac{1}{3}}/m_\pi$ is used for σ_{ν_e}

$$2\sigma_{\nu_e} = \frac{12^{\frac{2}{3}}}{m_\pi^2}. \tag{17}$$

$\bar{\nu}_e$ is detected by inverse beta decay and delayed signal of neutron capture. In this process, the lightest nucleus H i.e., proton can be a target and its wave function expands due to center of gravity effect [4]. As will be seen later, the diffraction term is proportional to σ_{ν_e} or $\sigma_{\bar{\nu}_e}$. According to these properties, the diffraction term for $\bar{\nu}_e$ can become larger than that for ν_e when a light nucleus contributes to the detection process. When C_nH_{2n+2} is used for scintillator, the size of wave packet is calculated from the ratio of proton between C and H, and is written as

$$2\sigma_{\bar{\nu}_e} = \frac{3}{4}\frac{12^{\frac{2}{3}}}{m_\pi^2} + \frac{1}{4}\left(\frac{m_e a_\infty}{m_p + m_e}\right)^2, \tag{18}$$

where m_e and m_p are masses of electron and proton, and a_∞ is Bohr radius. If the detector consists of a mixture of several materials, the wave packet size becomes the value averaged over the abundance ratio of materials.

The function $f(x)$ for in-coming state shows the propagating wave prepared in beam, and is determined by a mean free path,

$$l_\mu = \frac{1}{n\sigma_{\rm cross}}, \tag{19}$$

where n and $\sigma_{\rm cross}$ is density of scatterers and cross section respectively. The transition rate and average life-time of the velocity v are

$$\Gamma = n\sigma_{\rm cross} v = \frac{v}{l_\mu},\ \tau_{\rm int} = \frac{1}{\Gamma}. \tag{20}$$

For a charged particle, the mean free path is determined by the cross section of Coulomb scattering with atoms. The energy loss is also determined by the same cross section and is summarized in Ref. [6].

For a muon produced in a decay of pion from proton collision, the spatial size of proton is used. From the energy loss rates for several metals such as Pb, Fe, and others, a mean free path of proton of 1 GeV/c was estimated as $L_{\rm proton} = 50 - 100$ cm and at lower momentum of 2 MeV/c, $L_{\rm proton} = 10$ cm. The size of pion produced in high-energy proton collisions with target nucleus is computed using the above values of the proton and target size. In relativistic-energy region, particles have the speed of light and in the pion production process,

the size of pion, δx_π, is connected with those of the proton $\delta x_{\rm proton}$ in the form, $\frac{\delta x_{\rm proton}}{v_{\rm proton}} = \frac{\delta x_\pi}{v_\pi}$, $\delta x_\pi = \frac{v_\pi}{v_{\rm proton}} \delta x_{\rm proton} \approx \delta x_{\rm proton}$, where v_i is the speed of particle. Consequently pion's size of momentum 1 GeV/c or larger is given by $\delta x_\pi \approx 40 - 100$ cm. Since the muon is produced from pion decay, its size is determined by similar way. Muon's size is connected with the pion's size and their speeds, $\frac{\delta x_\pi}{v_\pi} = \frac{\delta x_\mu}{v_\mu}$, and is expressed in the form $\delta x_\mu = \frac{v_\mu}{v_\pi} \delta x_\pi$. For the relativistic particles, the speeds are almost the speed of light and their ratio is unity. So we have $\delta x_\mu = \delta x_\pi$. Hence, the size of the muon of the energy around 1GeV/c is given as $\delta x_\mu \approx 40 - 100$ cm.

μ^+ and μ^- decay in symmetric manner in vacuum with the mean life-time at rest, $\tau_\mu = 2.2 \times 10^{-6}$ sec. However, they have opposite charge and interact with atoms differently, hence behave in asymmetric manner in matter.

For the stopped μ^+, the wave functions in periodic potential of solid are extended waves of continuous energies. They are plane waves of phase shifts, and are extended in space. Thus μ^+ at rest, $v = 0$, is described by the wave function of large size. The stopped μ^- can form bound states, and their wave functions are localized of discrete energies. Thus μ^- at rest are described by the wave function of small sizes. Consequently, the decay of μ^+ at rest (μ^+DAR) is studied with the initial state of plane waves and the decay of μ^- at rest (μ^-DAR) is studied with the initial state of bound states. For both $\mu^\pm$ decays in flight ($\mu^\pm$ DIF), they are produced from decays of $\pi^\pm$ and retain coherence of same size of $\pi^\pm$. So it is good approximations to treat $\mu^\pm$DIF as plane waves [4].

III. THE ELECTRON NEUTRINO

$\bar{\nu}_e$ is identified by the inverse β process, and the geometry of muon decay at rest is shown in Fig. 2; cT is muon decay region, and D is detector. The length between decay region and detector denoted L is set to zero for simplicity in this section.

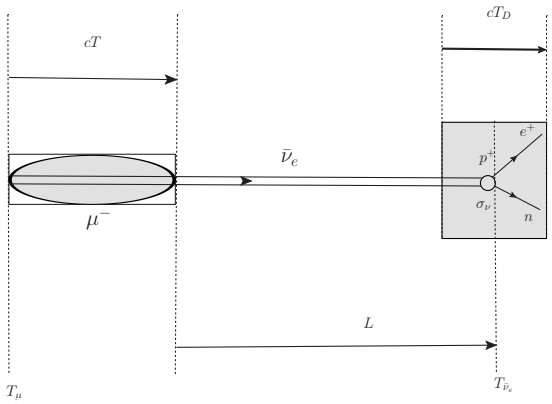

FIG. 2. The geometry of μ^- decay at rest is shown. In real experiments, a detector of cT_D m long is located away from decay region. However, in Sec. 3 we study a case where a detector is located in front of decay region, that is, $L = 0$ for simplicity.

A. Asymptotic spectrum and rate

The rate and spectrum of the electron neutrino at the asymptotic region, $T \to \infty$, are

$$\Gamma^0 = \frac{G_F^2 m_\mu^5}{192\pi^3}, \tag{21}$$

$$\frac{d\Gamma^0}{dE_{\nu_e}} = \frac{G_F^2}{2\pi^3} m_\mu^2 E_{\nu_e}^2 \left(1 - \frac{2E_{\nu_e}}{m_\mu}\right) \tag{22}$$

in the lowest order of G_F for the plane waves of the parent μ at rest and daughters. The electron mass and the radiative corrections were neglected in Eqs. (21) and (22).

B. Position dependent amplitude from $S[T]$

The matrix element of $S[T]$ for the case without neutrino flavor mixing is studied first for simplicity. We use the same notation for the particle and anti-particle; μ for μ^+ and μ^-, and so on, in the following. The amplitude from a wave packet of muon denoted as $|\mu\rangle$ to a final state of plane waves for e and ν_μ and a wave packet for ν_e $|e, \nu_\mu, \nu_e\rangle$ [13]

$$|\mu\rangle = |\vec{p}_\mu, \vec{X}_\mu, T_\mu\rangle, \ |e, \nu_\mu, \nu_e\rangle = |\vec{p}_e, \vec{p}_{\nu_\mu}, \vec{p}_{\nu_e}, \vec{X}_{\nu_e}, T_{\nu_e}\rangle \tag{23}$$

for not so large $|t - T_{\nu_e}|$ is

$$\mathcal{M} = \frac{G_F}{\sqrt{2}} 8 N_\mu^{-1} N_{\nu_e}^{-1} \varrho_\mu \varrho_e \varrho_{\nu_\mu} \varrho_{\nu_e} f I(\delta p),\ \delta p = p_\mu - p_e - p_{\nu_\mu} - p_{\nu_e}, \tag{24}$$

$$I(\delta p) = \int_{T_\mu}^{T_{\nu_e}} dt \int d\vec{x} e^{-i\delta\phi(x)} w(x, X_\mu; \sigma_\mu) w(x, X_{\nu_e}; \sigma_{\nu_e}),$$

$$f = \bar{u}(\vec{p}_{\nu_\mu}) \gamma_\rho (1 - \gamma_5) u(\vec{p}_\mu) \bar{u}(\vec{p}_e) \gamma^\rho (1 - \gamma_5) u(\vec{p}_{\nu_e}),$$

$$\delta\phi(x) = \phi_\mu(x, \vec{p}_\mu) - \phi_e(x, \vec{p}_e) - \phi_{\nu_\mu}(x, \vec{p}_{\nu_\mu}) - \phi_{\nu_e}(x, \vec{p}_{\nu_e}),$$

$$N_\mu = \left(\frac{\sigma_\mu}{\pi}\right)^{\frac{3}{4}},\ N_{\nu_e} = \left(\frac{\sigma_{\nu_e}}{\pi}\right)^{\frac{3}{4}},\ \varrho_\alpha = \left(\frac{m_\alpha}{(2\pi)^3 E_\alpha}\right)^{\frac{1}{2}}, \tag{25}$$

$$\phi_\alpha(x, \vec{k}_\alpha) = E(\vec{k}_\alpha)(t - T_\alpha) - \vec{k}_\alpha \cdot (\vec{x} - \vec{X}_\alpha),\ (\alpha = \mu, \nu_e), \tag{26}$$

$$\phi_\beta(x, \vec{p}_\beta) = E(\vec{p}_\beta) t - \vec{p}_\beta \cdot \vec{x},\ (\beta = e, \nu_\mu). \tag{27}$$

For larger $|t - T_{\nu_e}|$, the spreading effect of wave packet becomes non-negligible but as was shown in Ref. [4] for the pion decay, the final result is also almost the same in the muon decay. So the spreading is not expressed explicitly in the most places. At large $|t - T_{\nu_e}|$, the wave packet vanishes at $(t - T_{\nu_e})^2 - (\vec{x} - \vec{X}_{\nu_e}) \leq 0$ [5], but we ignore this effect in the present paper.

C. Probability

Averaging over the initial spin and summing over the final spins, we have the probability

$$P = \left(\frac{\pi^2}{\sigma_\mu \sigma_{\nu_e}}\right)^{\frac{3}{2}} \frac{2^8 G_F^2}{E_\mu (2\pi)^3} \int \frac{d\vec{p}_e d\vec{p}_{\nu_\mu} d\vec{X}_{\nu_e} d\vec{p}_{\nu_e}}{E_e E_{\nu_\mu} E_{\nu_e} (2\pi)^{12}} (p_\mu \cdot p_{\nu_e})(p_e \cdot p_{\nu_\mu}) \left| I(\delta p) \right|^2, \tag{28}$$

which is decomposed to the normal term, $T\Gamma^0$, and the diffraction term, $P^{(d)}$.

1. *Normal term*

The normal term, $T\Gamma^0$ in Eq. (28), where $T = T_{\nu_e} - T_\mu$, is

$$\begin{aligned} P^{\text{normal}} =& T \frac{(\sigma_\mu \sigma_{\nu_e})^{\frac{3}{2}}}{|\vec{v}_\mu - \vec{v}_{\nu_e}| (\sigma_\mu + \sigma_{\nu_e})} \frac{2^4 G_F^2}{E_\mu (2\pi)^7} \int \frac{d\vec{p}_e d\vec{p}_{\nu_\mu} d\vec{p}_{\nu_e}}{E_e E_{\nu_\mu} E_{\nu_e}} (p_\mu \cdot p_{\nu_e})(p_e \cdot p_{\nu_\mu}) \\ & \times \exp\left[-\frac{\sigma_\mu \sigma_{\nu_e}}{\sigma_\mu + \sigma_{\nu_e}} \delta\vec{p}^2 \right] \exp\left[-\frac{\sigma_\mu + \sigma_{\nu_e}}{(\vec{v}_\mu - \vec{v}_{\nu_e})^2} \left(\delta p^0 - \vec{v}_0 \cdot \delta\vec{p} \right)^2 \right] \end{aligned} \tag{29}$$

[3]. The condition $T \ll \tau_\mu$ is satisfied in all the case of experiments analyzed in the present paper. The case of $T \approx \tau_\mu$ is given in Appendix A.

2. Finite-size corrections: spectral representation

We write the probability, next, with the correlation function,

$$P = \frac{2^5 G_F^2}{(\sigma_\mu \sigma_{\nu_e})^{\frac{3}{2}} E_\mu} \int \frac{d\vec{X}_{\nu_e} d\vec{p}_{\nu_e}}{E_{\nu_e}(2\pi)^6} \int d^4x_1 d^4x_2 \Delta_{e,\nu_\mu}(\delta x) e^{ip_{\nu_e}\cdot\delta x} e^{-\frac{t_1+t_2}{2\tau_\mu}} \times \prod_i w(x_i, X_\mu; \sigma_\mu) w(x_i, X_{\nu_e}; \sigma_{\nu_e}), \tag{30}$$

$$\Delta_{e,\nu_\mu}(\delta x) = \frac{1}{(2\pi)^6} \int \frac{d\vec{p}_e d\vec{p}_{\nu_\mu}}{E_e E_{\nu_\mu}} (p_\mu \cdot p_{\nu_e})(p_e \cdot p_{\nu_\mu}) e^{i(p_e + p_{\nu_\mu} - p_\mu)\cdot\delta x}. \tag{31}$$

Substituting Appendix B, we have the integral representation of Jost, Lehmann and Dyson [14, 15],

$$\Delta_{e,\nu_\mu}(\delta x) = \frac{p_\mu \cdot p_{\nu_e}}{2(2\pi)^2} \int_{m_e^2} dm^2 \rho(m^2) i D^+(\delta t, \delta\vec{x}; p_\mu, m), \tag{32}$$

where

$$\rho(m^2) = m^2 - 2m_e^2 + \frac{m_e^4}{m^2}, \tag{33}$$

$$iD^+(\delta t, \delta\vec{x}; p_\mu, m) = \frac{1}{(2\pi)^3} \int d^4Q \delta(Q^2 - m^2) \theta(Q^0) e^{i(Q-p_\mu)\cdot\delta x}. \tag{34}$$

$iD^+(\delta t, \delta\vec{x}; p_\mu, m)$ is that of a relativistic particle of the mass m, and is given as

$m \le m_\mu$

$$\begin{aligned} iD^+(\delta t, \delta\vec{x}; p_\mu, m) \quad &= e^{-i\delta p_\mu\cdot\delta x} \frac{1}{(2\pi)^3} \int_{Q^0=0}^{Q^0=p_\mu^0} \frac{d\vec{Q}}{2Q^0} e^{iQ\cdot\delta x} + \frac{i}{4\pi}\delta(\lambda)\epsilon(\delta t) \\ &+ \sum_{n=0}^{\infty} \frac{1}{n!} \left(\frac{\partial}{\partial\tilde{m}^2}\right)^n \left(-ip_\mu \cdot \frac{\partial}{\partial\delta x}\right)^n i\tilde{D}^+(\delta t, \delta\vec{x}; i\tilde{m}), \end{aligned} \tag{35}$$

$m_\mu < m$

$$iD^+(\delta t, \delta\vec{x}; p_\mu, m) \quad = 0, \tag{36}$$

where $\tilde{D}^+(\delta t, \delta\vec{x}; i\tilde{m})$ is the sum of the Bessel functions. The power series in the above equation converges and the light-cone singularity appears only in the region [4],

$$2p_\mu \cdot p_{\nu_e} \le m_\mu^2 - m^2. \tag{37}$$

The singular part $i\frac{\epsilon(\delta t)}{4\pi}\delta(\lambda)$ in $iD^+(\delta t, \delta\vec{x}; p_\mu, m)$ and $\sigma_\mu \gg \sigma_{\nu_e}$, leads

$$\begin{aligned}
&\int d\vec{X}_{\nu_e} \int d^4x_1 d^4x_2 e^{ip_{\nu_e}\cdot\delta x} e^{-\frac{1}{4\sigma_\mu}(\delta\vec{x}-\vec{v}_\mu\delta t)^2 - \frac{1}{4\sigma_{\nu_e}}(\delta\vec{x}-\vec{v}_{\nu_e}\delta t)^2} i\frac{\epsilon(\delta t)}{4\pi}\delta(\lambda) \\
&\qquad \times \prod_{i=1,2} w(x_i, X_\mu; \sigma_\mu) w(x_i, X_{\nu_e}; \sigma_{\nu_e}) \\
&= \frac{i\sigma_{\nu_e}(\pi^2\sigma_\mu\sigma_{\nu_e})^{\frac{3}{2}}}{2} \int_0^T dt_1 dt_2 e^{-\frac{(\vec{v}_{\nu_e}-\vec{v}_\mu)^2\delta t^2}{4\sigma_\mu}} e^{-\frac{t_1+t_2}{2\tau_\mu}} \frac{e^{i(\omega_{\nu_e}\delta t)}}{\delta t},
\end{aligned} \tag{38}$$

where $\omega_{\nu_e} = \frac{m_{\nu_e}^2}{2E_{\nu_e}}$, and details and general cases of integral with $f(\delta x)$ are given in Appendix C. The integral in t_1 and t_2 in Eq. (38) becomes for two extremum cases,

$$0, \text{ for } \frac{4\sigma_\mu}{(\vec{v}_\mu - \vec{v}_{\nu_e})^2} = microscopic, \tag{39}$$

$$\tau_\mu \left\{\tilde{g}(\omega_{\nu_e}, T; \tau_\mu) - g(\omega_{\nu_e}, \infty; \tau_\mu)\right\}, \text{ for } \frac{4\sigma_\mu}{(\vec{v}_\mu - \vec{v}_{\nu_e})^2} = \infty, \tag{40}$$

where $\tilde{g}(\omega_{\nu_e}, T; \tau_\mu)$ and $g(\omega_{\nu_e}, \infty; \tau_\mu)$ are also given in Appendix C. The first term in the right-hand side of Eq. (40) behaves as $1/T$ at $\omega_{\nu_e} T \gg 1$, and the second term, and the first and third terms in Eq. (35) give the normal term.

For $\sigma_\mu \approx \infty$, the probability is written as

$$P = \frac{2G_F^2}{E_\mu} \int \frac{d\vec{p}_{\nu_e} p_\mu \cdot p_{\nu_e}}{E_{\nu_e}(2\pi)^5} \int dm^2 \rho(m^2) \left[\sigma_{\nu_e} \mathcal{C} \tilde{g}(\omega_{\nu_e}, T; \tau_\mu) + \text{“Normal”}\right], \tag{41}$$

where

$$\int_{m_e^2}^{m_\mu^2 - 2p_\mu\cdot p_{\nu_e}} dm^2 \rho(m^2) \simeq \frac{\left(m_\mu^2 - 2p_\mu\cdot p_{\nu_e}\right)^2}{2} \theta(m_\mu^2 - 2p_\mu \cdot p_{\nu_e}), \tag{42}$$

and $\mathcal{C}$ is constant in p_{ν_e} and given in Appendix C for various cases. In the above derivation, we used Eq. (37) and ignored m_e.

Finally we have

$$P = T\Gamma^0 + P^{(d)}, \tag{43}$$

$$P^{(d)} = \mathcal{C}\frac{G_F^2}{E_\mu} \int \frac{d\vec{p}_{\nu_e}}{E_{\nu_e}(2\pi)^5} (p_\mu \cdot p_{\nu_e})(m_\mu^2 - 2p_\mu\cdot p_{\nu_e})^2 \theta(m_\mu^2 - 2p_\mu\cdot p_{\nu_e}) \sigma_{\nu_e} \tilde{g}(\omega_{\nu_e}, T; \tau_\mu). \tag{44}$$

After the tedious calculations, we have

$$P^{(d)} = \frac{G_F^2}{(2\pi)^5 E_\mu}\left(\tilde{J}_1(p_\mu) + \tilde{J}_2(p_\mu)\right)$$
$$= \frac{G_F^2 \sigma_{\nu_e} \mathcal{C}}{(2\pi)^4 E_\mu |\vec{p}_\mu|}\left[\int_0^{E_{\min}} dE_{\nu_e} F_1(E_{\nu_e})\tilde{g}(\omega_{\nu_e}, T; \tau_\mu) + \int_{E_{\min}}^{E_{\max}} dE_{\nu_e} F_2(E_{\nu_e})\tilde{g}(\omega_{\nu_e}, T; \tau_\mu)\right]. \tag{45}$$

$$F_1(E_{\nu_e}) = E_{\nu_e}^2\left[E_{\nu_e}^2\left(p_\mu^{+4} - p_\mu^{-4}\right) - \frac{4}{3}E_{\nu_e} m_\mu^2\left(p_\mu^{+3} - p_\mu^{-3}\right) + \frac{m_\mu^4}{2}\left(p_\mu^{+2} - p_\mu^{-2}\right)\right] \tag{46}$$

$$F_2(E_{\nu_e}) = E_{\nu_e}^2\left[E_{\nu_e}^2\left\{p_\mu^{-4} - \left(\frac{m_\mu^2}{2E_{\nu_e}}\right)^4\right\} - \frac{4}{3}E_{\nu_e} m_\mu^2\left\{p_\mu^{-3} - \left(\frac{m_\mu^2}{2E_{\nu_e}}\right)^3\right\}\right.$$
$$\left. + \frac{m_\mu^4}{2}\left\{p_\mu^{-2} - \left(\frac{m_\mu^2}{2E_{\nu_e}}\right)^2\right\}\right].$$

In the above equations, the integral over the angle θ between the momenta of μ and ν_e is made by considering the convergence condition Eq. (37),

$$\cos\theta \leq \cos\theta_c = \frac{E_\mu}{|\vec{p}_\mu|} - \frac{m_\mu^2}{2|\vec{p}_\mu||\vec{p}_{\nu_e}|}. \tag{47}$$

D. Energy spectrum

1. *Diffraction component*

The energy spectrum of the diffraction component is given by

$$\frac{dP^{(d)}}{dE_{\nu_e}} = \frac{G_F^2 \sigma_{\nu_e} \mathcal{C}}{(2\pi)^4 E_\mu |\vec{p}_\mu|}[F_1(E_{\nu_e})\tilde{g}(\omega_{\nu_e}, T; \tau_\mu)\theta(E_{\min} - E_{\nu_e})$$
$$+ F_2(E_{\nu_e})\tilde{g}(\omega_{\nu_e}, T; \tau_\mu)\theta(E_{\max} - E_{\nu_e})\theta(E_{\nu_e} - E_{\min})]. \tag{48}$$

For the low-energy muon $|\vec{p}_\mu| \ll E_\mu \sim m_\mu$,

$$F_1(E_{\nu_e}) = |\vec{p}_\mu|\frac{m_\mu^7}{2}x^2(1-x)^2,\ F_2(E_{\nu_e}) = 0,\ x = \frac{2E_{\nu_e}}{m_\mu}, \tag{49}$$

Equation. (48) and the spectrum at asymptotic region, Eq. (22), are given in Fig. 3 for a suitable value of σ_{ν_e}. The value at at $cT = 1$ m indicates that the diffraction term $P^{(d)}$ is much larger than the normal term in magnitude, and that is about the same at $CT = 10$ m. Moreover the peak shifts to lower energies by an amount of around 20 MeV. This arises from the fact that the dominant part of $P^{(d)}$ comes from the large momentum states and is

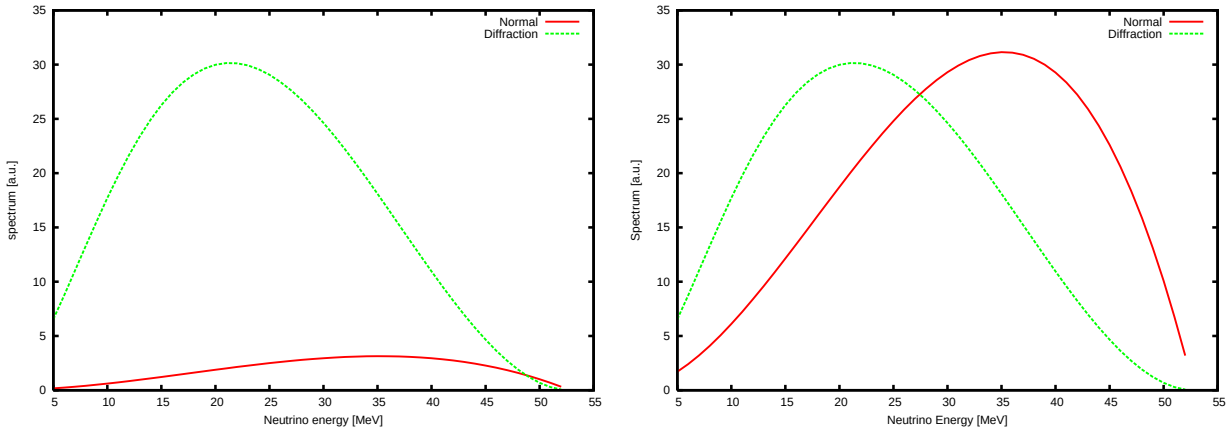

FIG. 3. (Color online) ν_e spectrum in μDAR. The red curve shows the normal component given in Eq. (50) and the green curve shows the diffraction component given in Eq. (48). $m_{\nu_e} = 0.08$ eV, and $2\sigma_{\nu_e} = 12^{\frac{2}{3}}/m_\pi^2$ (^{12}C carbon target) are used for numerical computation. Here, detector is located at $L = 0$. The left figure is for $cT = cT_D = 1$ and right one is for $cT = cT_D = 10$ m.

derived from those satisfying the condition Eq. (37). There is no precise data even for the electron in $x < 1/2$, by now, and it would be interesting to confirm this component. The effect is reduced if the muon is a small wave packet. Low-energy-negative muon in matter is trapped to an atom and forms a bound state of a small wave function, and the effect is reduced.

2. *Normal component*

From Eq. (22), the energy dependence of normal component of μDAR at asymptotic region is written as

$$\frac{dP^0}{dx} = \frac{G_F^2 m_\mu^5}{2(2\pi)^3} x^2(1-x)\tau_\mu(1 - e^{-\frac{T_D}{\tau_\mu}}), \tag{50}$$

where T_D is a depth of detector. For μDAR, the depth of the detector determines the time width. For μDIF, a decay region cT restricts the time width where μ exists. Those of suitable values according to experimental conditions are used. The normal component of transition rate or probability is independent of the size of wave packets from the completeness, but the energy spectrum depends on it and varies with the size. The spectrum for plane wave given in Eq. (22) was confirmed in the electron spectrum in the upper-energy region $x \geq 1/2$.

E. Mean life-time at a finite distance

The total probability becomes larger than the asymptotic value due to the diffraction component in small T, hence the average life-time measured by detecting the neutrino there becomes shorter than the asymptotic value, Eq. (21). At $T \to 0$, the diffraction term does not depend on σ_ν, and it may be possible to determine σ_ν experimentally by using this feature [13].

F. Mixing effect on diffraction term

The flavor oscillation in the particle-zone is described with the one-particle wave function, but that in the wave-zone is not. The mixing effect in $P^{(d)}$ is very different from usual flavor oscillation of Γ^0. That depends on m_ν and is sensitive to the difference of mass of the order of 0.1 eV or less [16]. Hereafter we study the effect caused by by the matrix $U_{\alpha,i}$.

With three mass eigen states of neutrino of m_{ν_i}, $i = 1 - 3$ and $U_{\alpha,i}$, the flavor neutrino fields $\nu_l(x)$ in Eq. (4) are the linear combination of the fields of three $\nu_i(x)$ having mass m_i as

$$\nu_l(x) = \sum_i U_{l,i}\nu_i(x),\ l = e,\ \mu, \tau, \tag{51}$$

where the best-fit values of mixing angles given in Ref. [6]

$$\sin^2 2\theta_{12} = 0.846 \pm 0.021, \tag{52}$$

$$\sin^2 2\theta_{23} = 0.999^{+0.001}_{-0.0018}\ \text{(normal hierarchy)},\ \sin^2 2\theta_{23} = 1.0000^{+0.000}_{-0.017}\ \text{(inverted)}, \tag{53}$$

$$\sin^2 2\theta_{13} = (9.3 \pm 0.8) \times 10^{-2}, \tag{54}$$

are used and CP violation phase $\delta_{CP} = 0$ is assumed. The amplitude for the anti-neutrino of flavor α to be detected in μ^+ decay ($\mu^+ \to \underline{\bar{\nu}_\mu} + e^+ + \nu_e$) is

$$\mathcal{M}_{\alpha,\mu} = \sum_i U_{\alpha,i}\mathcal{M}(\mu^+, i)U^*_{\mu,i}, \tag{55}$$

or the amplitude for the neutrino of flavor α' in μ^+ decay ($\mu^+ \to \bar{\nu}_\mu + e^+ + \underline{\nu_e}$) is

$$\mathcal{M}'_{\alpha',e} = \sum_i U_{\alpha',i}\mathcal{M}'(\mu^+, i)U^*_{e,i}. \tag{56}$$

Then, the amplitude for a flavor change from α to β is proportional to a new universal function $\tilde{g}_{\alpha,\beta}(\omega_{\nu_\alpha}, T; \tau_\mu)$ as

$$\mathcal{M}_{\alpha,\beta} \propto \tilde{g}_{\alpha,\beta}(\omega_{\nu_\beta}, T; \tau_\mu) = \sum_{i,j} U_{\beta,i} U^*_{\alpha,i} U^*_{\beta,j} U_{\alpha,j} \tilde{g}(\omega_i, \omega_j, T; \tau_\mu). \tag{57}$$

The function $\tilde{g}_{\alpha,\beta}(\omega_{\nu_\beta}, T; \tau_\mu)$ are summarized in Appendix C. They have the following features:

(1) $\tilde{g}_{e,e}(\omega_{\nu_e})$ and $\tilde{g}_{\mu,e}(\omega_{\nu_e})$ are almost constant at $T < 100$m of the magnitude sensitive to the absolute neutrino mass. So, there is a wide window where the absolute neutrino mass can be measured by using the finite-size corrections.

(2) $\tilde{g}_{\mu,e}(\omega_{\nu_e})$ is much smaller than $\tilde{g}_{e,e}(\omega_{\nu_e})$ but does not vanish and causes a new flavor changing effect on neutrino.

Implications of these effects will be discussed in the next section.

IV. IMPLICATIONS TO NEUTRINO EXPERIMENTS

We compare the probability of the events that neutrinos are detected with the experiments. At ground experiments, μ^+ (μ^-) is produced in π^+ (π^-) decay simultaneously with a ν_μ ($\bar{\nu}_\mu$), and decays to e^+ (e^-), $\bar{\nu}_\mu$ (ν_μ) and ν_e ($\bar{\nu}_e$). There are typical two types; one is the accelerator experiment that uses a neutrino beam from pion decay. In this case, both decays of high-energy π and μ are source of neutrinos. The other is the experiment that observes $\bar{\nu}_e$ or ν_μ appearance in μ^+ decay. In the latter, μ^+ is extracted and used as a source of neutrino, and π is not involved.

Hereafter, we focus only on μ^+ decay and study the above two types of experiments, and give predictions for future experiments. They would supply the absolute neutrino mass and the information on hierarchy of neutrino masses.

A. ν_e and $\bar{\nu}_\mu$ in μ^+ decay

1. μ^+ decay at rest (μ^+DAR)

In μ^+DAR, only ν_e is observable and $\bar{\nu}_\mu$ cannot be observed in charged current interactions. However, in order to distinguish back ground events or the flavor oscillation phenomena, spectrum of $\bar{\nu}_\mu$ is also important. Both ν_e and $\bar{\nu}_\mu$ have finite-size corrections, and the

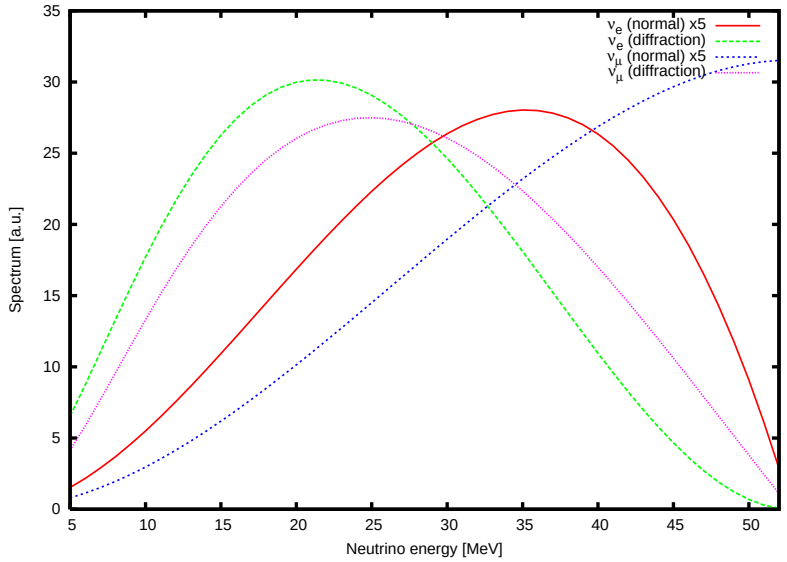

FIG. 4. (Color online) The spectra of normal and diffraction terms for ν_e and $\bar{\nu}_\mu$ in the μ^+ decay at rest are shown. The spectra of normal terms for ν_e (red) and $\bar{\nu}_\mu$ (blue) are different from those of ν_e (green) and $\bar{\nu}_\mu$ (magenta). These properties can be used to eliminate back ground events from μ^- decays, and so on. $m_{\nu_h} = 0.08$ eV, $\sigma_\nu = 12^{\frac{2}{3}}/m_\pi^2$, $cT = cT_D = 1.0$ m, and inverted hierarchy is assumed in numerical calculation.

spectra of normal and diffraction terms for $\bar{\nu}_\mu$ are

$$\frac{dP^0}{dE_{\bar{\nu}_\mu}} = \frac{G_F^2 m_\mu^2}{12\pi^3} E_{\bar{\nu}_\mu}^2 \left(3 - 4\frac{E_{\bar{\nu}_\mu}}{m_\mu}\right) \tau_\mu \left(1 - e^{-\frac{T_D}{\tau_\mu}}\right), \tag{58}$$

$$\frac{dP^{(d)}}{dE_{\bar{\nu}_\mu}} = \frac{G_F^2 m_\mu^2}{12\pi^3} \frac{E_{\bar{\nu}_\mu}^2 m_\mu^2 \sigma_{\bar{\nu}_\mu}}{4\pi} \left(1 - 2\frac{E_{\bar{\nu}_\mu}}{m_\mu}\right) \left(5 - 6\frac{E_{\bar{\nu}_\mu}}{m_\mu}\right) \tau_\mu \tilde{g}(\omega_{\bar{\nu}_\mu}, T; \tau_\mu), \tag{59}$$

and a ratio of them are

$$\begin{aligned} R(E_{\bar{\nu}_\mu}) &= \frac{dP^{(d)}}{dE_{\bar{\nu}_\mu}} \Big/ \frac{dP^0}{dE_{\bar{\nu}_\mu}} \\ &= \frac{m_\mu^2 \sigma_{\bar{\nu}_\mu}}{4\pi} \frac{\left(1 - 2\frac{E_{\bar{\nu}_\mu}}{m_\mu}\right)\left(5 - 6\frac{E_{\bar{\nu}_\mu}}{m_\mu}\right)}{3 - 4\frac{E_{\bar{\nu}_\mu}}{m_\mu}} \frac{\tilde{g}(\omega_{\bar{\nu}_\mu}, T; \tau_\mu)}{1 - e^{-\frac{T_D}{\tau_\mu}}}. \end{aligned} \tag{60}$$

As is the case with the spectrum of diffraction term for ν_e, the spectrum Eq. (59) gives lower energy components.

The spectra of diffraction and normal terms for ν_e are given in Eqs. (48) and (50) and ratio of them are

$$R(E_{\nu_e}) = \frac{\sigma_{\nu_e} m_\mu^2 \left(1 - \frac{2E_{\nu_e}}{m_\mu}\right)}{4\pi \left(1 - \exp[-T_D/\tau_\mu]\right)} \tilde{g}_{e,e}(\omega_{\nu_e}, T; \tau_\mu), \tag{61}$$

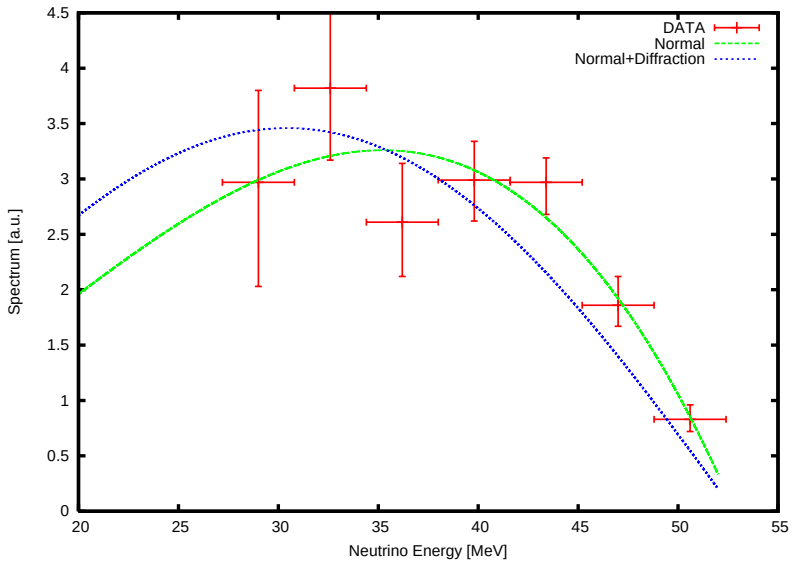

FIG. 5. (Color online) The spectra of normal and diffraction terms for ν_e are compared with KARMEN data. ν_e spectra of normal term is green curve and the sum of normal and diffraction terms is blue curve, and those of KARMEN experiment are crosses. Suitable parameters are chosen and relative magnitudes are shown.

Figure 4 shows the spectra Eqs. (48), (50), (58), and (59). The distinctive spectra of having peaks in the lower energy regions and the unique properties that the magnitude varies with T and σ_{ν_e} make it easy to distinguish them from the back ground events.

According to Fig. 4, the ratios Eqs. (60) and (61) are about 5 at $cT = 1$ m with $m_{\nu_h} = 0.08$ eV of inverted hierarchy. This value is quite large compared with that of π decay [16]: if it is possible to identify ν_e from μ^+DAR and collect sufficient statistics, it may be feasible to observe the finite-size correction as the excess of ν_e flux and measure the absolute neutrino mass. The spectrum from KARMEN experiment is compared with the normal and diffraction terms in Fig. 5. The statistics is not enough, and both theories are not in-consistent with the experiment.

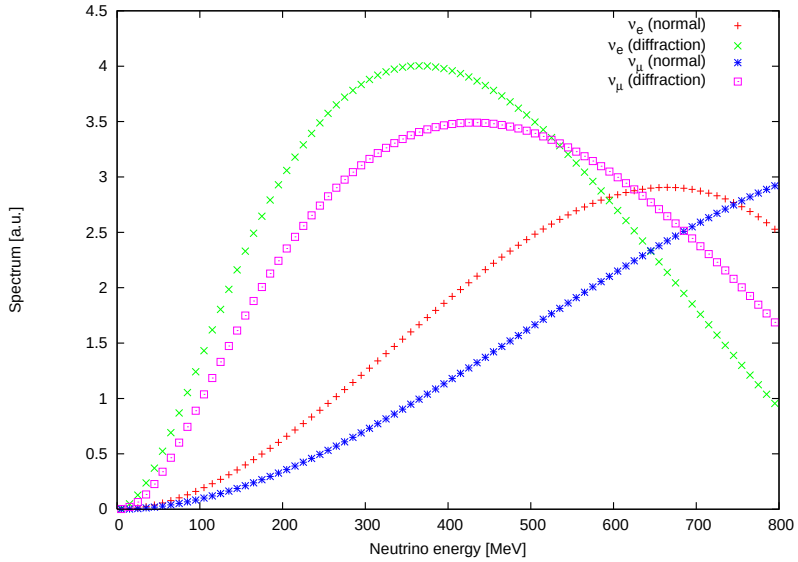

FIG. 6. (Color online) The spectra of the normal and diffraction terms for ν_e and $\bar{\nu}_\mu$ in μ^+DIF are shown. The spectra of the normal terms for ν_e (red) and $\bar{\nu}_\mu$ (blue) are different from those of ν_e (green) and $\bar{\nu}_\mu$ (magenta). These properties can be used to eliminate back ground events from μ^- decays, and so on. $m_{\nu_h} = 0.08$ eV, $\sigma_\nu = 12^{\frac{2}{3}}/m_\pi^2$, $cT = 200$ m, $\cos\theta = 1$, and $E_\mu = 1$ GeV are used, and inverted hierarchy is assumed in numerical calculation.

2. μ^+ decay in flight (μ^+DIF)

In μ^+DIF, the spectra of ν_e for the normal and diffraction terms are

$$\frac{d^2P^0_{\nu_e}}{dE_{\nu_e}d\cos\theta} = \frac{2G_F^2E_{\nu_e}^2}{(2\pi)^3E_\mu}(E_\mu - p_\mu\cos\theta)(m_\mu^2 - 2p_\mu\cdot p_{\nu_e})\gamma\tau_\mu\left(1-\exp\left[-\frac{T}{\gamma\tau_\mu}\right]\right), \tag{62}$$

$$\frac{d^2P^{(d)}_{\nu_e}}{dE_{\nu_e}d\cos\theta} = \frac{G_F^2E_{\nu_e}^2}{(2\pi)^4E_\mu}(E_\mu - p_\mu\cos\theta)(m_\mu^2 - 2p_\mu\cdot p_{\nu_e})^2\sigma_{\nu_e}\gamma\tau_\mu\tilde{g}_{e,e}(\omega_{\nu_e},T;\gamma\tau_\mu), \tag{63}$$

where θ is an angle between $\vec{p}_\mu$ and $\vec{p}_{\bar{\nu}_\mu}$, and $\gamma = E_\mu/m_\mu$, and those of $\bar{\nu}_\mu$ are

$$\frac{d^2P^0_{\bar{\nu}_\mu}}{dE_{\bar{\nu}_\mu}d\cos\theta} = \frac{G_F^2E_{\bar{\nu}_\mu}^2}{24\pi^3E_\mu}\left[(E_\mu - p_\mu\cos\theta)(3m_\mu^2 - 4E_{\bar{\nu}_\mu}(E_\mu - p_\mu\cos\theta))\right]$$
$$\times\gamma\tau_\mu\left(1-\exp\left[-\frac{T}{\gamma\tau_\mu}\right]\right), \tag{64}$$

$$\frac{d^2P^{(d)}_{\bar{\nu}_\mu}}{dE_{\bar{\nu}_\mu}d\cos\theta} = \frac{G_F^2}{24\pi^3E_\mu}\frac{E_{\bar{\nu}_\mu}^2}{4\pi}(E_\mu - p_\mu\cos\theta)(m_\mu^2 - 2E_{\bar{\nu}_\mu}(E_\mu - p_\mu\cos\theta))$$
$$\times(5m_\mu^2 - 6E_{\bar{\nu}_\mu}(E_\mu - p_\mu\cos\theta))\gamma\tau_\mu\sigma_{\bar{\nu}_\mu}\tilde{g}_{\mu,\mu}(\omega_{\bar{\nu}_\mu},T;\gamma\tau_\mu). \tag{65}$$

The ratios between normal and diffraction terms for ν_e and $\bar{\nu}_\mu$ are

$$R(E_{\nu_e},\cos\theta) = \frac{\sigma_{\nu_e}}{4\pi}(m_\mu^2 - 2E_{\nu_e}(E_\mu - p_\mu\cos\theta))\frac{\tilde{g}_{e,e}(\omega_{\nu_e},T;\gamma\tau_\mu)}{1-\exp[-T/\gamma\tau_\mu]}, \tag{66}$$

$$R(E_{\bar{\nu}_\mu},\cos\theta) = \frac{\sigma_{\bar{\nu}_\mu}}{4\pi}\frac{(m_\mu^2 - 2E_{\bar{\nu}_\mu}(E_\mu - p_\mu\cos\theta))(5m_\mu^2 - 6E_{\bar{\nu}_\mu}(E_\mu - p_\mu\cos\theta))}{3m_\mu^2 - 4E_{\bar{\nu}_\mu}(E_\mu - p_\mu\cos\theta)}\frac{\tilde{g}_{\mu,\mu}(\omega_{\bar{\nu}_\mu},T,\gamma\tau_\mu)}{(1-\exp[-T/\gamma\tau_\mu])}. \tag{67}$$

The spectra Eqs. (62)–(65) are shown in Fig. 6. They indicate that $R(E_{\bar{\nu}_\mu})$ and $R(E_{\nu_e})$ for on-axis $\bar{\nu}_\mu$ and ν_e are about unity with $E_\mu = 1$ GeV, $m_{\nu_h} = 0.08$ eV of inverted hierarchy, and σ_ν of nuclear size at $cT = 200$ m. Because this effect is clear and unique, this may be observed at high-energy neutrino experiments, even for the small neutrino flux. This will be compared with existing experimental results in the next section.

3. Excess of electron neutrino in accelerator experiments

To study the flavor oscillation phenomena, accelerator neutrino experiments use a neutrino beam produced by π decays and search an excess in electron neutrino mode. In π^+ decay, ν_e is produced in processes

$$\pi^+ \to \mu^+ + \nu_\mu, \tag{68}$$

$$\mu^+ \to e^+ + \bar{\nu}_\mu + \underline{\nu_e}, \tag{69}$$

$$\to e^+ + \underline{\nu_e}, \tag{70}$$

and has two sources. Because the probability to detect neutrinos in both decays are subject of the finite-size corrections, it is necessary to include them. The correction to ν_e in π^+ decay has been compared with the existing data of MiniBooNE [16, 19], and the whole corrections are compared here. Since μ^+ is the second particle produced by π^+ decay, its decay region is reduced by the distance where the parent π^+ travels until its decay. This effect of pion's finite life-time is also included to compute the finite-size correction.

MiniBooNE experiment [19] reported the appearance of ν_e and $\bar{\nu}_e$ in ν_μ or $\bar{\nu}_\mu$ beam produced by $\pi^\pm$ decay. The previous analysis used only the normal mode, but does not include the diffraction mode. We include the diffraction mode obtained under the MiniBooNE experimental condition. The correction to ν_e from π^+ decay, Eq. (70), was found before in Ref. [16], and that of ν_e from μ^+, Eq. (69), is given in Fig. 7. Figure 7 indicates that our

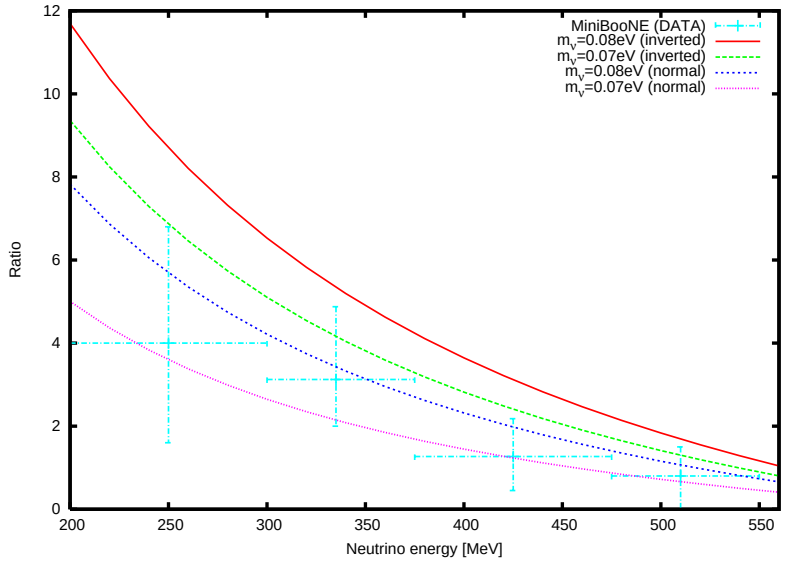

FIG. 7. (Color online) $P_{\nu_e}^{(d)}/P_{\nu_e}^{(0)}(\mu)$ is compared with the MiniBooNE data (light-blue) including statistic and systematic errors [19]. For numerical calculation, $m_{\nu_h} = 0.07$ eV (green: inverted, magenta: normal), $m_{\nu_h} = 0.08$ eV (red: inverted, blue: normal), $E_\mu = 670$ MeV, and $E_\pi = 1.15$ GeV are used.

numerical results of ratio between normal and diffraction modes agree with the data. This shows, furthermore, that the finite-size correction in μ^+ decay dominates in ν_e events at MiniBooNE experiments, and is sensitive to the absolute mass value of neutrino and mass hierarchy. Our results are consistent within errors of the experiment and Monte Carlo simulation with the absolute neutrino mass values of $m_{\nu_h} = 0.07 - 0.08$ eV. This is consistent with our previous results [16]. Figure 8 shows the energy dependence of ratio $P_{\nu_e}^{(d)}/P_{\nu_e}^{(0)}$ of our theory at MicroBooNE experiment [20]. In this experiment, the neutrino beam is the same as that of MiniBooNE. MicroBooNE detector is smaller than that of MiniBooNE but the target nucleus is ^{40}Ar, whose size is much larger than ^{12}C and the finite-size correction also becomes large. With using two different lengths of decay region and sufficient statistics, not only the mass hierarchy but also the absolute neutrino mass can be determined.

B. Neutrino flavor changes through diffraction

The diffraction causes a flavor change at short-distance distinct from the ordinary flavor oscillation of Γ_0. In μ^+DAR, Eq.(3), $\bar{\nu}_e$ does not exist in the final state in the absence of mixing. The mixing is necessary and there are two cases that $\bar{\nu}_e$ appears and is detected

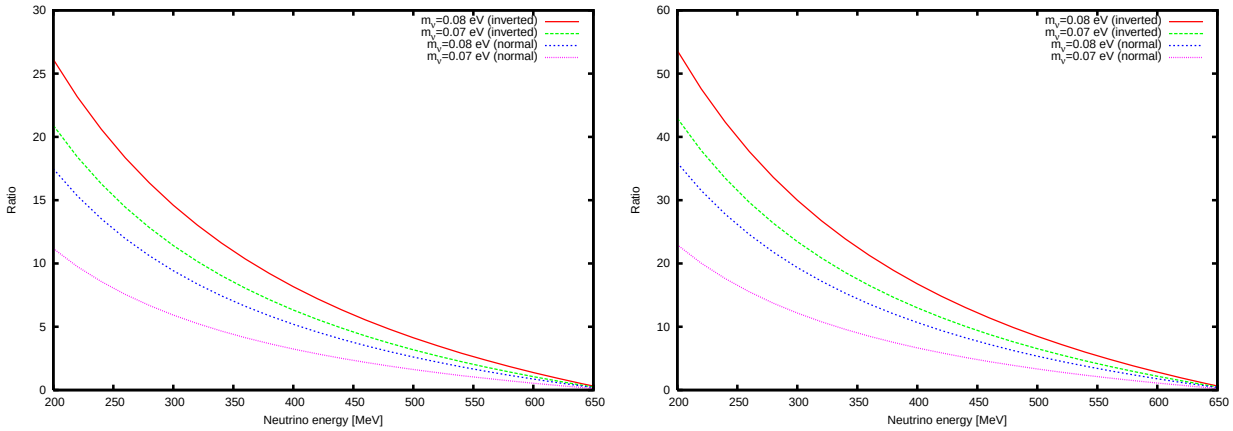

FIG. 8. (Color online) The energy dependences of the ratio $P_{\nu_e}^{(d)}/P_{\nu_e}^{0}$ of our theory for MicroBooNE [20] setup are shown. The left figure is of $cT = 50$ m and right one is of 25 m. For numerical calculation, $m_{\nu_h} = 0.07$ eV (green: inverted, magenta: normal), $m_{\nu_h} = 0.08$ eV (red: inverted, green: normal), $E_\mu = 670$ MeV, and $E_\pi = 1.15$ GeV are used. Target nucleus is ^{40}Ar.

at near-detectors of $L \sim 10 - 100$ m. One is a flavor oscillation through Γ_0 and another is from the mixing through $P^{(d)}$. The former requires a large Δm^2 of the order of 1 eV^2, which is beyond the masses of three neutrinos. Hence at least one new kind of neutrino that does not have electro-magnetic or weak interaction, so-called sterile neutrino [17, 18] is necessary there. However the latter requires no additional neutrino, and has the energy spectra different from that of flavor oscillation. Accordingly it is possible to distinguish them experimentally.

In μ^+DIF, both ν_μ and $\bar{\nu}_\mu$ can be detected in charged current interactions, because the energies of neutrinos are high enough to create muons. Their energy spectra are very different in two interpretations. For $P^{(d)}$, not only $\bar{\nu}_\mu$ but also ν_μ gets an excess in its flux, but for the Γ_0, that is not the case. Two can be distinguished clearly, hence μ^+DIF experiments are desirable.

1. LSND and KARMEN (μ^+DAR)

Two experiments of similar geometry made with μ^+DAR to search the $\bar{\nu}_e$ appearance at near detectors, LSND [21] and KARMEN [22] are inconsistent under the neutrino-flavor-oscillation hypothesis. However that is not the case for the flavor change through $P^{(d)}$. LSND

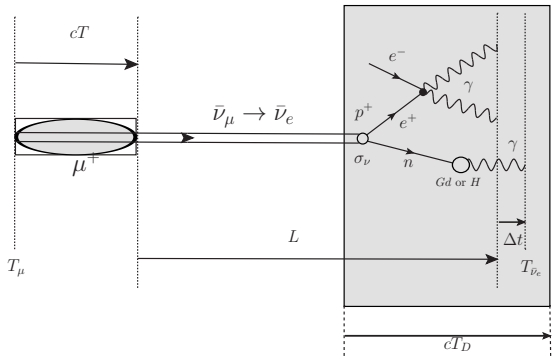

FIG. 9. Space-time geometry of the detection of $\bar{\nu}_e$ through inverse-beta process with the delayed coincidence in μ^+DAR is shown. T is the time width where μ^+ and its decay products can overlap. L is length between the decay region and the detector that is used in flavor oscillation formula. Δt is time difference between the photon signals of positron and neutron capture that is used for event selection in KARMEN experiment.

reported the event excess that is explained by the parameters $(\Delta m^2_{LSND}, \sin^2 2\theta_{LSND}) = (1.2\ \mathrm{eV}^2, 0.003)$ as the best-fit, whereas no excess was observed in KARMEN. The parameters and results are summarized in Table I, and the geometry of the μ^+DAR experiment is shown in Fig. 9. The important difference between them is the time difference denoted as Δt between the prompt signal from positron in anti-beta decay and delayed signal from neutron capture. KARMEN required $5 < \Delta t < 300$ μs but LSND used likelyfood-ratio instead of Δt. This makes essential difference in the boundary conditions, which we examine later. We compute the probability of the flavor change thorough $P^{(d)}$ under experimental conditions of LSND and KARMEN and find that they are in accord with experiments.

The energy spectra from two processes are given by

$$\frac{dP^{(d)}}{dE_{\bar{\nu}_e}} = \frac{G_F^2 m_\mu^2 \tau_\mu}{12\pi^3} E_{\bar{\nu}_e}^2 \frac{m_\mu^2 \sigma_{\bar{\nu}_e}}{8\pi} \left(1 - 2\frac{E_{\bar{\nu}_e}}{m_\mu}\right) \left(5 - 6\frac{E_{\bar{\nu}_e}}{m_\mu}\right) \tilde{g}_{\mu,e}(\omega_{\bar{\nu}_e}, T; \tau_\mu), \tag{71}$$

$$\frac{dP^{\mathrm{osc}}}{dE_{\bar{\nu}_e}} = \frac{G_F^2 m_\mu^2 \tau_\mu}{12\pi^3} E_{\bar{\nu}_e}^2 \left(3 - 4\frac{E_{\bar{\nu}_e}}{m_\mu}\right) \left(e^{-\frac{T_\mu}{\tau_\mu}} - e^{-\frac{(T_\mu + T_D)}{\tau_\mu}}\right) \sin^2 2\theta \sin\left(1.27\frac{\Delta m^2}{E_\nu} L\right). \tag{72}$$

The former has no free parameter, but the latter has new mass-squared difference δm^2. The ratio $\frac{dP^d/dE}{dP^{\mathrm{osc}}/dE}$ of LSND and KARMEN are shown in Fig. 10. The parameters shown in Table I are used to calculate the ratios numerically. From this figure, $P^{(d)}$ for LSND parameters

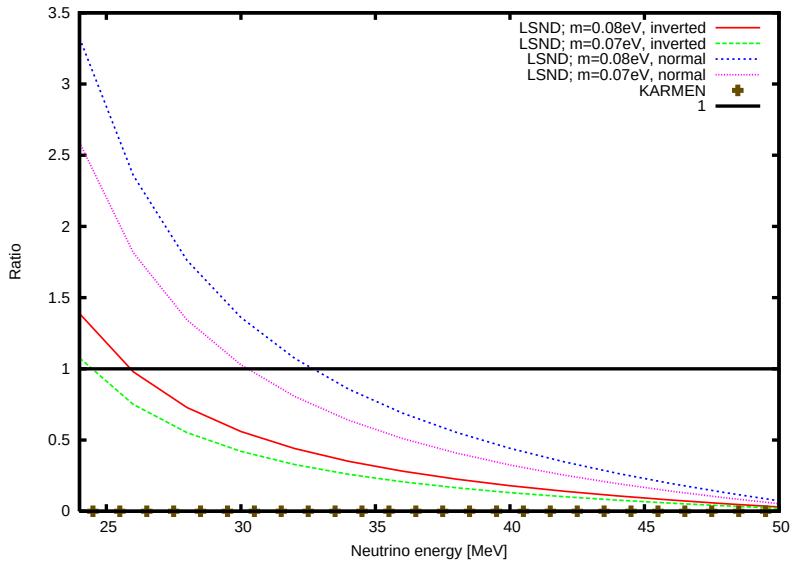

FIG. 10. (Color online) The ratios $\frac{dP^{(d)}/dE}{dP^{\rm osc}/dE}$ are shown. For LSND, $T_\mu = 0$, $cT = 0.8$ m ($T \sim 2.5$ ns), $cT_D = 8.3$ m, $L = 29.8$ m, $\sigma_{\bar{\nu}_e}^{\rm LSND}$ of $C_{2n}H_{2n+2}$, $\Delta m^2_{LSND} = 1.2$ eV^2, and $\sin^2 2\theta_{LSND} = 0.003$ are used. Red curve shows inverted hierarchy of $m_{\nu_h} = 0.08$ eV, green curve shows inverted of $m_{\nu_h} = 0.07$ eV, blue curve shows normal hierarchy of $m_{\nu_h} = 0.08$ eV, and magenta curve shows normal of $m_{\nu_h} = 0.07$ eV. For KARMEN, $T_\mu = 0.3$ μs, $\Delta t = 5$ μs, $cT = 0.3$ m ($T \sim 1.0$ ns), $cT_D = 3.5$ m, $m_{\nu_h} = 0.08$ eV of inverted hierarchy, $L = 17.7$ m, angle between proton beam and detector $\theta = 100°$, $\sigma_{\bar{\nu}_e}^{\rm KARMEN}$, $\Delta m^2_{LSND} = 1.2$ eV^2 and $\sin^2 2\theta_{LSND} = 0.003$ are used. A geometry for μ^+DAR is shown in Fig. 9 and a relation between T and θ is given in Appendix C 3.

is in the same order of the magnitude with flavor oscillation with LSND best-fit parameters while that for KARMEN vanishes. This difference results from methods of event selection they used.

The diffraction term emerges when the wave functions of parent and daughters overlap. This constrains the wave's positions. Following Fig. 9, the detector is located away from the muon decay region and the time region of the overlap is defined as $T = T_{\bar{\nu}_e} - T_\mu - L/c$ for μ^+DAR geometry. If the cut on time difference between photons from positron and those from neutron, Δt, is not used for event selection, the overlapping region T is determined by the initial and final times and agrees with the size of beam stop. The diffraction term, then, is automatically included into the event of $\bar{\nu}_e$. Now, when the time difference is used for the cut, the overlapping region is modified by Δt as $T = T_{\bar{\nu}_e} - T_\mu - L/c - \Delta t$. Then, only in case of $T > 0$, the waves overlap and the events include the diffraction term.

	LSND	KARMEN
Size of beam stop (D×W×H)	1 m×0.2 m×0.2 m	0.5 m× 0.25 m×0.25 m
L	29.8 m	17.7 m
Δt	No	5 μs$< \Delta t <$ 300 μs
Scintillator	CH_2	$C_nH_{2n+2}(75\%) + C_9H_{12}(25\%)$
$E_{\bar{\nu}_e}$	36(20)–60 MeV	16–50 MeV
Primary positron time window	No, $T_\mu = 0$	0.6 μs $< T_\mu <$ 10 μs
T_D, Depth of detector	8.3 m	3.5 m
Detector angle	10°	100°
$\bar{\nu}_e$ event excess	87.9±22.4±6.0	No excess
Best fit Δm^2 and $\sin^2\theta$	$\Delta m^2 = 1.2$ eV^2, $\sin^2\theta = 0.003$	None

TABLE I. Parameters and results of LSND and KARMEN.

KARMEN selected and used the events satisfying $\Delta t > 5$ μs and the events of $\Delta t < 5$ μs are excluded. Our estimation shows that the diffraction components occurs with the velocity of light in the region $\Delta t < 5$ μs. Whereas LSND did not cut the events, and all the events are included. Consequently the diffraction is included in LSND but not in KARMEN. Thus the disagreement between those two experiments that seems to be difficult to interpret as flavor oscillation can be understood. In addition, if the events for $\Delta t < T$ are included, $\bar{\nu}_e$ excess must be be seen in KARMEN. Δt dependence of ratio are given in Fig. 11. The magnitude of $P^{(\mathrm{d})}$ is approximately ten times larger than that of LSND because L of KARMEN is shorter than that of LSND. An indication may appear as a sharp peak in small Δt region in Ref. [22].

According to above analyses, both two experimental results of LSND and KARMEN can be explained with the finite-size corrections, and are consistent with the previous result of LSND πDIF [16]. Furthermore, with more precise energy spectrum and suitable selection criteria, it is possible to confirm the excess of $\bar{\nu}_e$ at near-detector as diffraction.

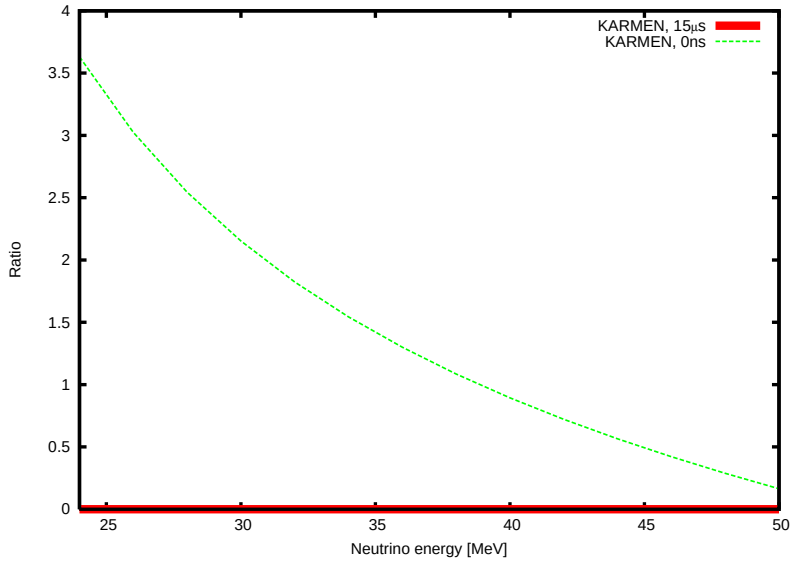

FIG. 11. (Color online) The Δt dependence of ratio for KARMEN. $\Delta t = 0$ ns (green), and $\Delta t = 15\mu$s (red). We use $m_{\nu_h} = 0.08$ eV of inverted hierarchy and all other parameters are same with Fig. 10.

2. *Future experiments of μ^+DAR and μ^+DIF*

There are two possible experiments to confirm the excess of flux of neutrino from μ^+ decay as the finite-size correction. One is a $\bar{\nu}_e$ appearance experiment with μ^+DAR [24]. The other is a ν_μ appearance and $\bar{\nu}_\mu$ disappearance with μ^+DIF [25]. Here, we give predictions for future experiments of both cases.

1. μ^+DAR

In μ^+DAR experiments, $\bar{\nu}_e$ spectrum is given by Eq. (71). Without requiring the double coincidence condition of Δt, the ratio between $\bar{\nu}_e$ and $\bar{\nu}_\mu$ spectra is written as

$$R_{\bar{\nu}_e}(E_\nu) = \frac{m_\mu^2 \sigma_{\bar{\nu}_e}}{8\pi} \frac{\left(1 - 2\frac{E_\nu}{m_\mu}\right)\left(5 - 6\frac{E_\nu}{m_\mu}\right)}{\left(3 - 4\frac{E_\nu}{m_\mu}\right)\left(e^{-\frac{T_\mu}{\tau_\mu}} - e^{-\frac{T_\mu + T_D}{\tau_\mu}}\right)} \tilde{g}_{\mu,e}(\omega_{\bar{\nu}_e}, T; \tau_\mu). \tag{73}$$

This is the simplest value under ideal conditions. The value for an experimental setup [24] is shown in Fig. 12, where cT, the size of beam stop, is 1 m, $T_\mu = 1$ μs, $cT_D = 3.4$ m, and $\sigma_{\bar{\nu}_e}$ is of $C_{2n}H_{2n+2}$ in the liquid scintillator. The magnitude compared with the expected $\bar{\nu}_e$ appearance by the simple flavor oscillation with one sterile neutrino is found in the ratio,

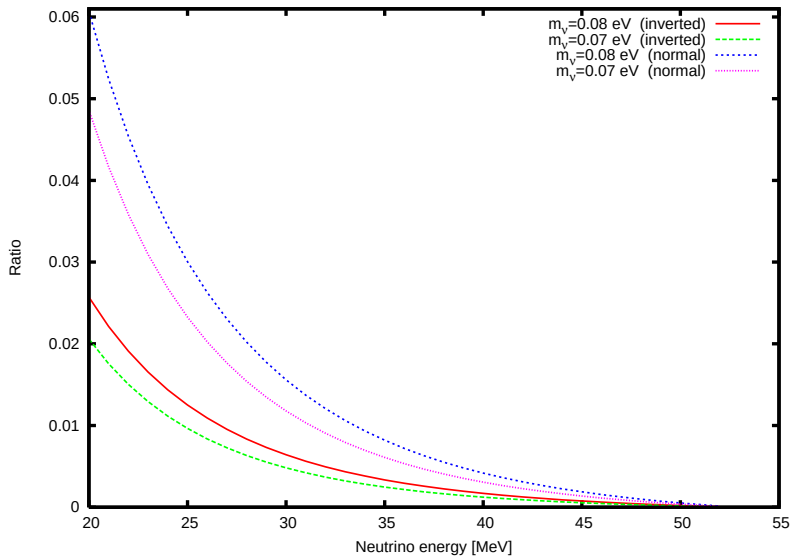

FIG. 12. (Color online) The ratios $\frac{dP^{(d)}_{\bar{\nu}_e}/dE}{dP^{0}_{\bar{\nu}_\mu}/dE}$, Eq. (73), for μ^+DAR are shown, where $T_\mu = 1$ μs, $cT = 1.0$ m, $L = 17.0$m, and $\sigma_{\bar{\nu}_e} = 7.3$ of $C_{2n}H_{2n+2}$ and $cT_D = 3.4$ m are used [24]. Red curve shows inverted hierarchy of $m_{\nu_h} = 0.08$ eV, green curve shows inverted of $m_{\nu_h} = 0.07$ eV, blue curve shows normal hierarchy of $m_{\nu_h} = 0.08$ eV, and magenta curve shows normal of $m_{\nu_h} = 0.07$ eV.

$\frac{dP^d/dE}{dP^{\rm osc}/dE}$,

$$R^{\rm osc}_{\bar{\nu}_e}(E_\nu) = \frac{m_\mu^2 \sigma_{\bar{\nu}_e}}{8\pi} \frac{\left(1-2\frac{E_\nu}{m_\mu}\right)\left(5-6\frac{E_\nu}{m_\mu}\right)\tilde{g}_{\mu,e}(\omega_{\bar{\nu}_e}, T; \tau_\mu)}{\left(3-4\frac{E_\nu}{m_\mu}\right)\left(e^{-\frac{T_\mu}{\tau_\mu}} - e^{-\frac{T_\mu+T_D}{\tau_\mu}}\right)\sin^2 2\theta_{\mu e}\sin^2\left(1.27\frac{\Delta m^2 41}{E_\nu}L\right)}. \tag{74}$$

Figure 13 shows the ratio Eq. (74), where experimental parameters are same with Fig. (12) and parameters of sterile neutrino are [18]

$$\Delta m^2_{41} = 0.9 \text{ eV}^2,\ U_{e4} = 0.15,\ U_{\mu 4} = 0.17, \tag{75}$$

$$\sin^2\theta_{\mu e} = 4\left|U_{\mu 4}U_{er}\right|^2,\ \sin^2\theta_{\mu\mu} = 4\left|U_{\mu 4}\right|^2\left(1-\left|U_{\mu 4}\right|^2\right). \tag{76}$$

These values are also used in next μ^+DIF case. According to Figs. 12 and 13, the magnitude of $\bar{\nu}_e$ appearance through the finite-size correction can be almost same with or larger than that of the flavor oscillation with the sterile neutrinos. Furthermore, the effect is sensitive to the absolute neutrino mass and the mass hierarchy of neutrino.

2. μ^+ DIF

In μ^+DIF experiment, an appearance of ν_μ ($\nu_e \to \nu_\mu$) from ν_e and a disappearance of $\bar{\nu}_\mu$ ($\bar{\nu}_\mu \to \bar{\nu}_e$) will be searched since the flavor oscillation with sterile neutrinos are kept in mind.

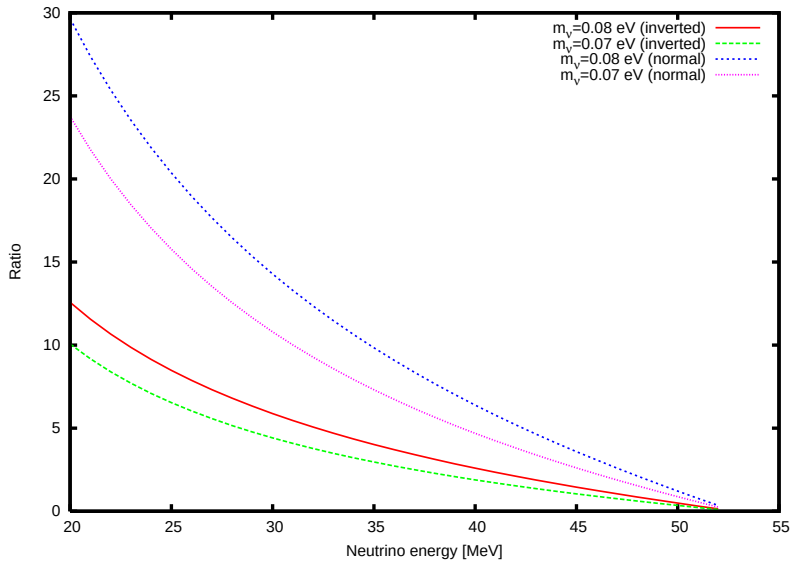

FIG. 13. (Color online) The ratios $\frac{dP^{(d)}_{\bar{\nu}_e}/dE}{dP^{osc}_{\bar{\nu}_e}/dE}$, Eq. (74), for μ^+DAR are shown, where $T_\mu = 1$ μs, $cT = 1.0$ m, $L = 17.0$ m, $cT_D = 3.4$ m, and $\sigma_{\bar{\nu}_e} = 7.3$ of $C_{2n}H_{2n+2}$ and are used [24]. Red curve shows the ratio of the inverted hierarchy with $m_{\nu_h} = 0.08$ eV, green curve shows that of the inverted hierarchy with $m_{\nu_h} = 0.07$ eV, blue curve shows the ratio of the normal hierarchy with $m_{\nu_h} = 0.08$ eV, and magenta curve shows the ratio of the normal hierarchy with $m_{\nu_h} = 0.07$ eV.

However, the finite-size corrections provide appearance of ν_μ and $\bar{\nu}_\mu$, and their magnitude and spectra are very different from those of sterile neutrinos. Using Eqs. (62) – (65), the ratios $\frac{P^{(d)}_{\nu_\mu}(E_\nu)}{P^{osc}_{\nu_\mu}(E_\nu)}$ and $\frac{P^{(d)}_{\bar{\nu}_\mu}(E_\nu)}{P^{osc}_{\bar{\nu}_\mu}(E_\nu)}$ are written as

$$R_{\nu_\mu}(E_\nu, \cos\theta) = \frac{\sigma_{\nu_\mu}(m_\mu^2 - 2E_\nu(E_\mu - p_\mu\cos\theta))\tilde{g}_{e,\mu}(\omega_\nu, T; \gamma\tau_\mu)}{2\pi\left(\exp\left[-\frac{T_\mu}{\gamma\tau_\mu}\right] - \exp\left[-\frac{T_\mu+T}{\gamma\tau_\mu}\right]\right)\sin^2 2\theta_{\mu e}\sin^2\left(1.27\frac{\Delta m^2_{41}}{E_\nu}L\right)}, \tag{77}$$

$$R_{\bar{\nu}_\mu}(E_\nu, \cos\theta) = \frac{\sigma_{\bar{\nu}_\mu}(m_\mu^2 - 2E_\nu(E_\mu - p_\mu\cos\theta))\tilde{g}_{e,\mu}(\omega_\nu, T; \gamma\tau_\mu)}{2\pi\left(\exp\left[-\frac{T_\mu}{\gamma\tau_\mu}\right] - \exp\left[-\frac{T_\mu+T}{\gamma\tau_\mu}\right]\right)\left(1 - \sin^2 2\theta_{\mu\mu}\sin^2\left(1.27\frac{\Delta m^2_{41}}{E_\nu}L\right)\right)}, \tag{78}$$

and that of $\bar{\nu}_\mu$ is given by Eq. (67). Eqs. (66) and (67) are given in Figs. 14 and 15. The target nucleus is ^{56}Fe and parameters given in Eqs. (75) and (76) are used. The ratio of ν_μ appearance at $L = 20$ m is very large. This is because T dependences are different in normal and diffraction terms. The normal term is very small at $T \ll \gamma\tau_\mu$ and P^0 increases with T, but the diffraction term $P^{(d)}$ is constant in T. In addition, the oscillation length with $\Delta m^2_{41} = 0.9$ eV^2 at $E_\nu = 1$ GeV is 800–900 m and the effect of the flavor oscillation is not significant at $L = 20$ m. Then, 10^3 larger magnitude of ν_μ appearance through the finite-size correction at $L = 20$ m is a natural consequence with the nature of diffraction term.

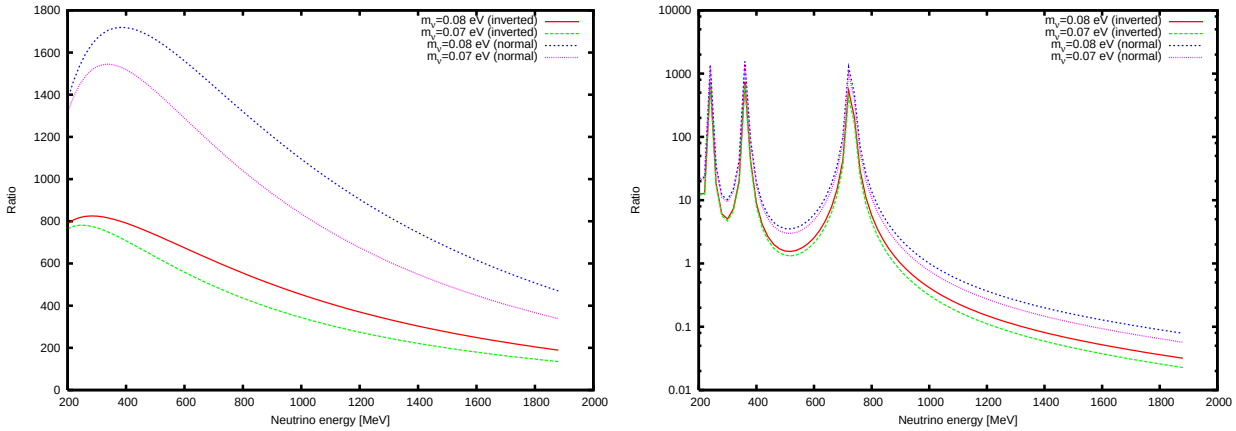

FIG. 14. (Color online) The ratios of ν_μ appearance $\frac{dP^{(d)}_{\nu_\mu}/dE_\nu}{dP^{osc}_{\nu_\mu}/dE_\nu}$, Eq. (74), for μ^+DIF are shown, where $T_\mu = 0$ μs, $cT = 226.0$ m, $L = 20.0$ m (Left) and $L = 2000.0$ m (Right), and σ_{ν_μ} = of ^{56}Fe and $\cos\theta = 1$ are used [25]. Red curve shows the ratio of the inverted hierarchy with $m_{\nu_h} = 0.08$ eV, green curve shows that of the inverted hierarchy with $m_{\nu_h} = 0.07$ eV, blue curve shows the ratio of the normal hierarchy with $m_{\nu_h} = 0.08$ eV, and magenta curve shows the ratio of the normal hierarchy with $m_{\nu_h} = 0.07$ eV. In the right figure, there are three sharp peaks because the denominator oscillates in energy and becomes very small.

Then, the relative magnitude between them becomes very large of order 10^3 at $cT = 226$ m $\ll \gamma\tau_\mu$ at $E_\mu = 3$ GeV.

The ratio of ν_μ appearance at $L = 2000$ m has three peaks because the numerator $dP^{(d)}_{\nu_\mu}/dE_\nu$ varies uniformly in energy and the denominator $dP^{osc}_{\nu_\mu}/dE_\nu$ oscillates in energy and becomes very small at certain energies.

V. SUMMARY

In this paper, we studied the diffraction term $P^{(d)}$ for muon decay in $T \leq \tau_\mu$, using the S-matrix $S[T]$ that satisfies the boundary conditions at finite T. In this region, the many-body wave function is the superposition of the parent and decay products, and the overlapping waves have the finite interaction energies and cause the kinetic energy distinct from that of the initial state. The diffraction term $P^{(d)}$ thus appears and the probability shows the non-uniform behavior, which is probed with the final state expressed by the wave packets. Using wave packets [5, 11], the space-time positions and momenta of particles were treated simultaneously, and the position dependent probability was computed.

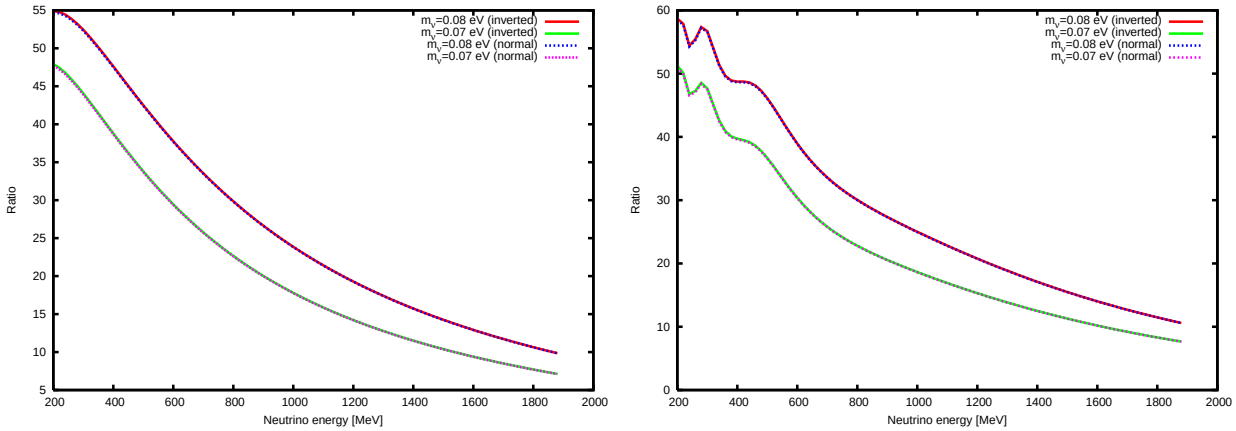

FIG. 15. (Color online) The ratios of excess and disappearance of $\bar{\nu}_\mu$, $\frac{dP^{(d)}_{\bar{\nu}_\mu}/dE}{dP^{osc}_{\bar{\nu}_\mu}/dE}$, Eq. (74), for μ^+DIF are shown, where $T_\mu = 0$ μs, $cT = 226.0$ m, $L = 20$ m (Left) and $L = 2000$ m (Right), and $\sigma_{\bar{\nu}_\mu}$ = of ^{56}Fe and $\cos\theta = 1$ are used [25]. Red curve shows the ratio of the inverted hierarchy with $m_{\nu_h} = 0.08$ eV, green curve shows that of the inverted hierarchy with $m_{\nu_h} = 0.07$ eV, blue curve shows the ratio of the normal hierarchy with $m_{\nu_h} = 0.08$ eV, and magenta curve shows the ratio of the normal hierarchy with $m_{\nu_h} = 0.07$ eV.

The constructive interference peculiar to relativistic waves found in the pion-two-body decay gives the more significant effects in the muon decay, due to large life-time and phase space of three particles. Because the diffraction term $P^{(d)}$ holds the wave-like properties, the neutrino flavor mixing modifies the probability in the different way from the standard mixing formula derived from Γ_0. The total probabilities thus computed agree with the experiments. The excess of neutrino flux at finite distance is as large as the asymptotic value, and the value is lager than that of the normal mode of neutrino in pion decay, which are the consequence of the longer life-time and the larger phase space. The experiments of LSND, MiniBooNE, and KARMEN have different geometries and the $P^{(d)}$ reflects the geometry. Hence, the experiments seemingly inconsistent each other if $P^{(d)}$ were not considered, become consistent when $P^{(d)}$ is included. Thus the experiments become to agree each other and with the theory only when the diffraction terms are included.

Thus the finite-size corrections are important and lead us to new physical quantities which can be measured directly. They give the significant contributions to the transition probability, hence play the important roles in the muon decays. Furthermore, because the neutrino spectrum from the diffraction term is sensitive to the absolute neutrino masses,

future precision experiments will be able to determine the absolute neutrino mass.

In this paper, it is shown that the quantum interference effect modifies the neutrino spectra in the muon decays at the finite distance. Since the boundary condition is a key for the effect, the higher-order corrections do not modify the result. The case in which the muon is described in small wave packet and other phenomena where the finite-size corrections play important roles will be presented in separate publication.

ACKNOWLEDGMENTS

This work was partially supported by a Grant-in-Aid for Scientific Research (Grant No. 24340043). Authors thank Dr. Kobayashi, Dr. Nishikawa, and Dr. Maruyama for useful discussions on the near-detector of T2K experiment, Dr. Asai, Dr. Kobayashi, Dr. Mori, and Dr. Yamada for useful discussions on interferences, Dr. Kinoshita and Dr. Nio for useful discussions on muon g–2 experiment.

Appendix A: Life-time effect on normal term

In $T \approx \tau_\mu$, the muon's life-time cannot be ignored and we have

$$\begin{aligned}\left|I^{\rm normal}(\delta p)\right|^2 = &\left(\frac{2\pi\sigma_\mu\sigma_{\nu_e}}{\sigma_\mu+\sigma_{\nu_e}}\right)^3 \exp\left[-\frac{\sigma_\mu\sigma_{\nu_e}}{(\sigma_\mu+\sigma_{\nu_e})}\delta\vec{p}^{\,2} - \frac{\left(\tilde{\vec{X}}_\mu - \tilde{\vec{X}}_{\nu_e}\right)^2}{(\sigma_\mu+\sigma_{\nu_e})}\right] \\ &\times \int dt_1 dt_2\, e^{-\frac{t_1+t_2}{\tau_\mu}+i\left(\delta p^0 - \vec{v}_0\cdot\delta\vec{p}\right)(t_1-t_2)} \\ &\times \exp\left[\frac{(\vec{v}_{\nu_e}-\vec{v}_\mu)\cdot\left(\tilde{\vec{X}}_{\nu_e}-\tilde{\vec{X}}_\mu\right)}{\sigma_\mu+\sigma_{\nu_e}}(t_1+t_2) - \frac{(\vec{v}_{\nu_e}-\vec{v}_\mu)^2}{2(\sigma_\mu+\sigma_{\nu_e})}(t_1^2+t_2^2)\right]. \qquad \text{(A1)}\end{aligned}$$

Integrating over $\vec{X}_{\nu_e}$,

$$\begin{aligned}\int d\vec{X}_{\nu_e}\left|I^{\rm normal}(\delta p)\right|^2 = &\, 16\frac{\pi^5\left(\sigma_\mu\sigma_{\nu_e}\right)^{\frac{3}{2}}}{(\sigma_\mu+\sigma_{\nu_e})|\vec{v}_{\nu_e}-\vec{v}_\mu|}\exp\left[-\frac{\sigma_\mu+\sigma_{\nu_e}}{(\vec{v}_{\nu_e}-\vec{v}_\mu)^2}\left(\delta p^0-\vec{v}_0\cdot\delta\vec{p}\right)^2\right] \\ &\times\exp\left[-\frac{\sigma_\mu\sigma_{\nu_e}}{\sigma_\mu+\sigma_{\nu_e}}\delta\vec{p}^{\,2}\right]\frac{\tau_\mu}{2}\left(1-e^{-\frac{2T}{\tau_\mu}}\right), \qquad \text{(A2)}\end{aligned}$$

for the wave packets of

$$\sqrt{\frac{\sigma_\mu+\sigma_{\nu_e}}{(\vec{v}_\mu-\vec{v}_{\nu_e})^2}} \ll \tau_\mu, T. \qquad \text{(A3)}$$

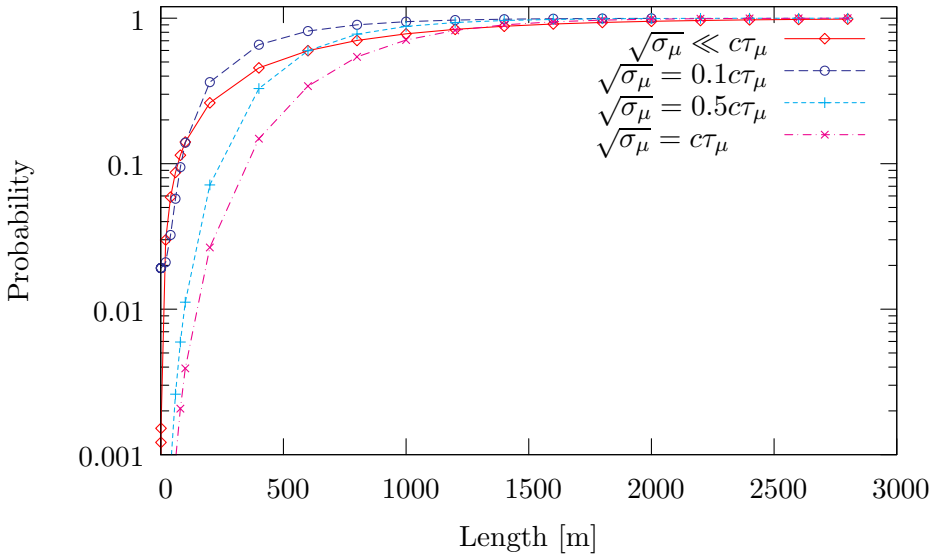

FIG. 16. (Color online) The σ_μ dependence of the probability of μDAR normalized to 1 at $T = \infty$. The probabilities computed with plane waves (asymptotic value) (red), $\sqrt{\sigma_\mu} = 0.1c\tau_\mu$ (deep blue), $\sqrt{\sigma_\mu} = 0.5c\tau_\mu$ (light blue), and $\sqrt{\sigma_\mu} = c\tau_\mu$ are given. We assume $\sigma_\mu \gg \sigma_{\nu_e}$. Deviations from simple exponential decay are significant at $L < c\tau_\mu$.

Outside Eq. (A3), the probability from normal term are computed numerically. The numerical result for μDAR is shown in Fig. 16.

Appendix B: Light-cone singularity

The light-cone singularities used are partly given in many textbooks and in Ref. [3, 4] , and new formulae used in this paper are summarized briefly.

(1) $D^+(\delta t, \delta\vec{x}; m)$ and $D^+(\delta t, \delta\vec{x}; m)$ are single particle correlation functions of the real mass and imaginary mass.

(2) The correlation function $D^+(\delta t, \delta\vec{x}; p, m)$ of an external momentum p is written as $D^+(\delta t, \delta\vec{x}; p, m) = e^{-ip\cdot\delta x} D^+(\delta t, \delta\vec{x}, m)$, $p^2 = m_0^2$. or $D^+(\delta t, \delta\vec{x}; p, m) = D^+_\infty(\delta t, \delta\vec{x}; p, m) +$

$D^+_{\rm finite}(\delta t, \delta\vec{x}; p, m)$. The latter is decomposed further

$$D^+_\infty(\delta t, \delta\vec{x}; p, m) = D_m(\xi)\, D^+_\infty(\delta t, \delta\vec{x}; i\tilde{m}), \tag{B1}$$

$$\tilde{m} = \sqrt{m_0^2 - m^2},\ \xi = -2ip\cdot\frac{\partial}{\partial\delta x},\ D_m(\xi) = \sum_{l=0}\frac{\xi^l}{l!}\left(\frac{\partial}{\partial\tilde{m}^2}\right)^l,$$

$$D_m(\xi)\, D^+_\infty(\delta t, \delta\vec{x}; i\tilde{m}) = \frac{\epsilon(\delta t)}{4\pi}\delta(\lambda) + D_m(\xi)\left[-\frac{\tilde{m}}{8\pi\sqrt{-\lambda}}\theta(-\lambda)\Big\{N_1\left(\tilde{m}\sqrt{-\lambda}\right) - i\epsilon(\delta t)J_1\left(\tilde{m}\sqrt{-\lambda}\right)\Big\} + \theta(\lambda)\frac{\tilde{m}}{4\pi^2\sqrt{\lambda}}K_1\left(\tilde{m}\sqrt{\lambda}\right)\right]. \tag{B2}$$

The light-cone singularity of $D^+_\infty(\delta t, \delta\vec{x}; p, m)$ is independent of p and m and exists in the region expressed in Eq. (37) of the text.

The integral over the region $-p_0 \le r_0 \le 0$ is written as,

$$D^+_{\rm finite}(\delta t, \delta\vec{x}; p, m) = \frac{1}{i(2\pi)^3}\int\frac{d\vec{q}}{E(\vec{q})}e^{i(q-p)\cdot\delta x}\theta(p_0 - E(\vec{q})). \tag{B3}$$

For $\tilde{m}^2 < 0$, $D^+(\delta t, \delta\vec{x}; p, m) = 0$.

(3) $D^+(\delta t, \delta\vec{x}; p, m)_{\alpha_1,\alpha_2,\cdots}$ of many-body states are expressed with the mass spectrum, $\rho(m^2)$, as

$$\int dm^2\rho(m^2)D^+(\delta t, \delta\vec{x}; p, m), \tag{B4}$$

$$\rho(m^2) = \int d(\text{phase space})\delta\left(m^2 - \left(\sum_l p_l\right)^2\right).$$

For two particles

$$\Delta_{e,\nu_\mu}(\delta x) = \frac{1}{(2\pi)^6}\int_{-\infty}^{\infty}\frac{d\vec{p}_e d\vec{p}_{\nu_\mu}}{E_e E_{\nu_\mu}}(p_\mu\cdot p_{\nu_e})(p_e\cdot p_{\nu_\mu})e^{i(p_e+p_{\nu_\mu}-p_\mu)\cdot\delta x}, \tag{B5}$$

$$= \frac{p_\mu\cdot p_{\nu_e}}{2(2\pi)^2}\int dm^2\left(m^2 - 2m_e^2 + \frac{m_e^4}{m^2}\right)iD^+(\delta t, \delta\vec{x}; p_\mu, m).$$

$$\Delta_{\nu_\mu,\nu_e}(\delta x) = \frac{1}{(2\pi)^6}\int_{-\infty}^{\infty}\frac{d\vec{p}_{\nu_\mu} d\vec{p}_{\nu_e}}{E_{\nu_\mu} E_{\nu_e}}(p_\mu\cdot p_{\nu_e})(p_e\cdot p_{\nu_\mu})e^{i(p_{\nu_\mu}+p_{\nu_e}-p_\mu)\cdot\delta x}, \tag{B6}$$

$$= \frac{i}{12(2\pi)^2}\int dm^2\left(m^2(p_\mu\cdot p_e) + 2p_\mu\cdot\left(p_\mu - i\frac{\partial}{\partial\delta x}\right)p_e\cdot\left(p_\mu - i\frac{\partial}{\partial\delta x}\right)\right) \times D^+(\delta t, \delta\vec{x}; p_\mu, m). \tag{B7}$$

Appendix C: Universal function $\tilde{g}(\omega, T; \tau_\mu)$

The integral over the coordinates x_1, x_2 and $\vec{X}_{\nu_e}$ is written as

$$\begin{aligned}
&\int d\vec{X}_{\nu_e} \int d^4x_1 d^4x_2 e^{ip_{\nu_e}\cdot\delta x} f(\delta x) \prod_{i=1,2} w(x_i, X_\mu; \sigma_\mu) w(x_i, X_{\nu_e}; \sigma_{\nu_e}) e^{-\frac{t_1+t_2}{\tau_\mu}} \\
&= \left(\frac{\pi\sigma_\mu\sigma_{\nu_e}}{\sigma_\mu+\sigma_{\nu_e}}\right)^{\frac{3}{2}} \int d\vec{X}_{\nu_e} e^{-\frac{\left(\tilde{\vec{X}}_\mu - \tilde{\vec{X}}_{\nu_e}\right)_T^2}{\sigma_\mu+\sigma_{\nu_e}}} \int dt_1 dt_2 d\delta\vec{x}\, e^{ip_{\nu_e}\cdot\delta x} e^{-\frac{1}{4\sigma_\mu}(\delta\vec{x}-\vec{v}_\mu\delta t)^2 - \frac{1}{4\sigma_{\nu_e}}(\delta\vec{x}-\vec{v}_{\nu_e}\delta t)^2} \\
&\times e^{-\frac{t_1+t_2}{\tau_\mu}} \exp\left[-\frac{(\vec{v}_\mu-\vec{v}_{\nu_e})^2}{\sigma_\mu+\sigma_{\nu_e}}\left(\frac{t_1+t_2}{2}-\tilde{T}_L\right)^2\right] f(\delta x), \qquad \text{(C1)} \\
&\tilde{T}_L = \frac{(\vec{v}_\mu-\vec{v}_{\nu_e})\cdot\left(\tilde{\vec{X}}_\mu - \tilde{\vec{X}}_{\nu_e}\right)}{(\vec{v}_\mu-\vec{v}_{\nu_e})^2},
\end{aligned}$$

and using Gaussian approximation for integration in $\vec{X}_{\nu_e}$, we have

$$\left(\pi^2\sigma_\mu\sigma_{\nu_e}\right)^{\frac{3}{2}} \int dt_1 dt_2 d\delta\vec{x}\, e^{ip_{\nu_e}\cdot\delta x} e^{-\frac{1}{4\sigma_\mu}(\delta\vec{x}-\vec{v}_\mu\delta t)^2 - \frac{1}{4\sigma_{\nu_e}}(\delta\vec{x}-\vec{v}_{\nu_e}\delta t)^2} e^{-\frac{t_1+t_2}{2\tau_\mu}} f(\delta x). \qquad \text{(C2)}$$

For $f(x) = i\frac{\epsilon(\delta t)}{4\pi}\delta(\lambda)$, integral in Eq. (C2) is written as

$$\begin{aligned}
&\int dt_1 dt_2 d\delta\vec{x} e^{ip_{\nu_e}\cdot\delta x} e^{-\frac{1}{4\sigma_\mu}(\delta\vec{x}-\vec{v}_\mu\delta t)^2 - \frac{1}{4\sigma_{\nu_e}}(\delta\vec{x}-\vec{v}_{\nu_e}\delta t)^2} \frac{i}{4\pi}\delta(\lambda)\epsilon(\delta t) e^{-\frac{t_1+t_2}{2\tau_\mu}} \\
&= \int_0^T dt_1 dt_2\, e^{-\frac{(\vec{v}_\mu-\vec{v}_{\nu_e})^2\delta t^2}{4\sigma_\mu}} \int d\vec{r} e^{ip_{\nu_e}\cdot\delta x} e^{-\frac{(\vec{r}-\vec{v}_{\nu_e}\delta t)^2}{4\sigma_{\nu_e}}} \frac{i}{4\pi}\delta(\lambda)\epsilon(\delta t) e^{-\frac{t_1+t_2}{2\tau_\mu}} \\
&\simeq \frac{i}{2}\sigma_{\nu_e} \int_0^T dt_1 dt_2 e^{-\frac{(\vec{v}_\mu-\vec{v}_{\nu_e})^2}{4\sigma_\mu}\delta t^2} e^{-\frac{(1-|\vec{v}_{\nu_e}|)^2}{4\sigma_{\nu_e}}\delta t^2} \frac{e^{i\omega_{\nu_e}\delta t}}{\delta t} e^{-\frac{t_1+t_2}{2\tau_\mu}}, \qquad \text{(C3)}
\end{aligned}$$

where $\omega_{\nu_e} = \frac{m_{\nu_e}^2}{2E_{\nu_e}}$, and $\sigma_{\nu_e}|\vec{p}_{\nu_e}| \ll T$ is used. Due to the small mass of neutrino, $e^{-\frac{(1-|\vec{v}_{\nu_e}|)^2}{4\sigma_{\nu_e}}} \approx 1$ but this suppression factor cannot be ignored for massive particles. The case for $\sigma_\mu \to \infty$ is summarized first. In this limit, the integral over t_1 and t_2 is generally written as $\mathcal{C}g(\omega_\nu, T; \tau_\mu)$ where $g(\omega_\nu, T; \tau_\mu)$ is dimension-less function and $\mathcal{C}$ is constant in ω_ν. Since $g(\omega_\nu, \infty; \tau_\mu)$ is cancelled with the term from J_{regular}, it is convenient to define $\tilde{g}(\omega_\nu, T; \tau_\mu) = g(\omega_\nu, T; \tau_\mu) - g(\omega_\nu, \infty; \tau_\mu)$. This new universal function $\tilde{g}(\omega_\nu, T; \tau_\mu)$ determines the behavior of the finite-size correction.

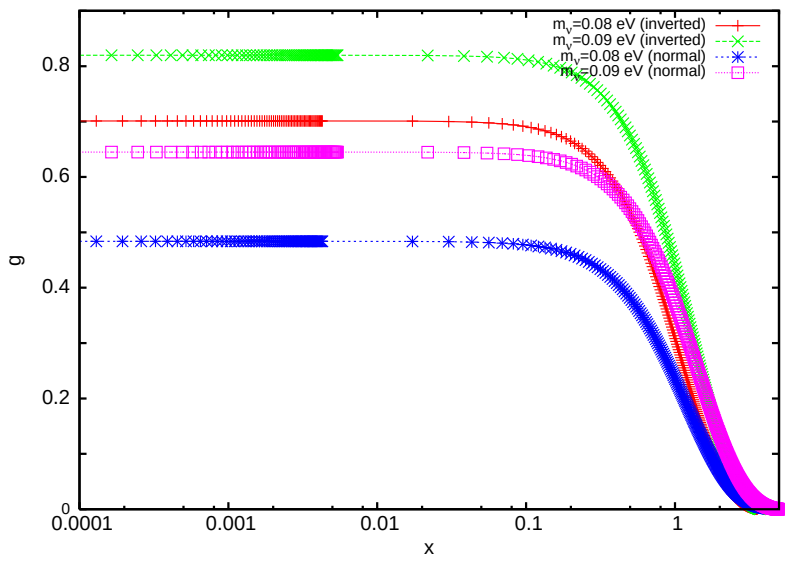

FIG. 17. (Color online) $\tilde{g}_{e,e}(\omega_{\nu_e}, T; \tau_\mu)$ of including flavor mixing, Eq. (C8), is shown. The horizontal axis is $x = \omega_{\nu_h} T$, where $\omega_{\nu_h} = \frac{m^2_{\nu_h}}{2E_{\nu_e}}$, m_{ν_h} is the mass of the heaviest neutrino. Color difference represent differences of mass values of $m_{nu_h} = 0.09$ eV (green: inverted hierarchy, magenta: normal) and $m_{\nu_h} = 0.08$ eV (red: inverted, blue: normal).

1. General form of $\tilde{g}(\omega_\nu, T; \tau_\mu)$

a. *Without mixing*

The universal function without mixing;

$$\begin{aligned} \mathcal{C}g(\omega_\nu, T; \tau_\mu) &= \frac{i}{2}\int_0^T dt_1 dt_2 \frac{e^{i\omega_\nu(t_1-t_2)}}{t_1-t_2} e^{-\frac{t_1+t_2}{2\tau_\mu}} \\ &= -\tau_\mu \int_0^T dt \frac{\sin(\omega_\nu t)}{t}\left(e^{-\frac{t}{2\tau_\mu}} - e^{-\frac{1}{2\tau_\mu}(2T-t)}\right), \end{aligned} \tag{C4}$$

where $t_+ = \frac{t_1+t_2}{2}$, $t_- = t_1 - t_2$, $\mathcal{C} = \tau_\mu$ and

$$g(\omega_\nu, \infty; \tau_\mu) = -\arctan(2\omega_\nu\tau_\mu). \tag{C5}$$

Then,

$$\tilde{g}(\omega_\nu, T; \tau_\mu) = \arctan(2\omega_\nu\tau_\mu) - \int_0^T dt \frac{\sin(\omega_\nu t)}{t}\left(e^{-\frac{t}{2\tau_\mu}} - e^{-\frac{1}{2\tau_\mu}(2T-t)}\right). \tag{C6}$$

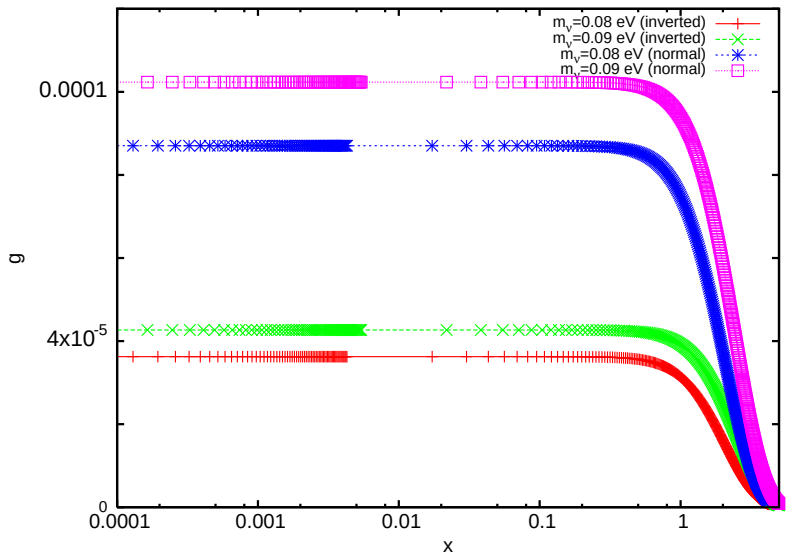

FIG. 18. (Color online) $\tilde{g}_{\mu,e}(\omega_{\nu_e}, T; \tau_\mu)$ of including flavor mixing, Eq. (C8), is shown. The horizontal axis is $x = \omega_{\nu_h} T$, where $\omega_{\nu_h} = \frac{m^2_{\nu_h}}{2E_{\nu_e}}$, m_{ν_h} is the mass of the heaviest neutrino. Color difference represent differences of mass values of $m_{nu_h} = 0.09$ eV (green: inverted hierarchy, magenta: normal) and $m_{\nu_h} = 0.08$ eV (red: inverted, blue: normal).

b. Mixing case

Originally, the light-cone singularity is computed with mass eigen state. Because flavor states of neutrino are superpositions of mass eigen states, the mixing matrix should be included to the diffraction terms. With mass eigen states of m_i and m_j, we have

$$\mathcal{C}g(\omega_i, \omega_j, \infty; \tau_\mu) = \frac{\tau_\mu}{1+\tau_\mu^2(\omega_i-\omega_j)^2}\left[-\frac{1}{2}(\arctan(2\omega_i\tau_\mu)+\arctan(2\omega_j\tau_\mu)) + \frac{\tau_\mu(\omega_i-\omega_j)}{4}\left[-\log(1+4\omega_j^2\tau_\mu^2)+\log(1+4\omega_i^2\tau_\mu^2)\right]\right]. \quad \text{(C7)}$$

Combining the mixing matrix and neutrino mass m_i with the diffraction term, the universal function is written as

$$\tilde{g}_{\alpha,\beta}(\omega_{\nu_\beta}, T; \tau_\mu) = \sum_{i,j} U_{\beta,i} U^*_{\alpha,i} U^*_{\beta,j} U_{\alpha,j} (g(\omega_i, \omega_j, T; \tau_\mu) - g(\omega_i, \omega_j, \infty; \tau_\mu)), \quad \text{(C8)}$$

and shown in Figs. 17 and 18 as functions of $x = \omega_\nu T$. According to those figures, $\tilde{g}_{\alpha,\beta}(\omega_{\nu_e}, T; \tau_\mu)$ is sensitive to the absolute neutrino mass and mass hierarchy and causes observable effects discussed in the text. The value of x is 0.0006 or 0.0007 for $cT = 1$ m, $m_{\nu_2} = 0.08$ eV, and $m_{\nu_2} = 0.09$ eV, and is 0.08 for $cT = 100$ m, $m_{\nu_2} = 0.08$ eV, and

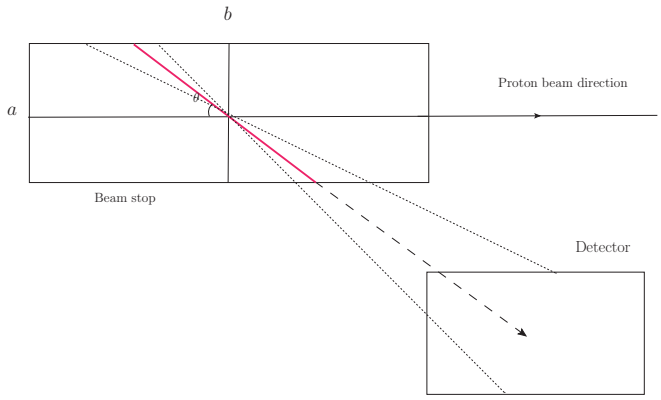

FIG. 19. (Color online) Angle dependence of overlapping region (red line) for μ^+DAR. It depends on the position and size of detector.

$m_{\nu_2} = 0.09$ eV, respectively, and $\tilde{g}_{e,e}(\omega_{\nu_e})$ and $\tilde{g}_{\mu,e}(\omega_{\nu_e})$ are almost constant at $T < 100$ m but the magnitude is sensitive to the absolute neutrino mass. So, there is a wide window where the absolute neutrino mass can be measured by using the finite-size corrections. Furthermore, $\tilde{g}_{\mu,e}(\omega_{\nu_e})$ is much smaller than $\tilde{g}_{e,e}(\omega_{\nu_e})$ but does not vanish and causes a new flavor changing effect on neutrino. Implications of this effect will be discussed in the next section, and more details about $\tilde{g}_{\alpha,\beta}$ are given in Appendix C.

2. Large life-time and T

For $\omega T \gg 1$, the universal function Eq. (C6) behaves as

$$\tilde{g}(\omega, T; \tau) \propto \frac{1}{\omega T}, \quad \omega\tau \approx 1 \tag{C9}$$

$$\tilde{g}(\omega, T; \tau) \sim \frac{2}{\omega T}, \quad \tau \to \infty. \tag{C10}$$

3. Angle dependence of overlapping region T

For μ^+DAR, the region where parent and daughters overlap is sensitive to the geometry of experiments and diffraction term depends on the angle between a beam axis and detector, even if the decay is spherically symmetric. Following Fig. 19, angle dependence region

denoted as T in the text is written as

$$T = \begin{cases} \frac{2a}{\cos\left(\frac{\pi}{2}-\theta\right)} \text{ for } 0 \leq \cos\theta < \frac{b}{\sqrt{a^2+b^2}} \\ \frac{2b}{\cos\theta} \text{ for } \frac{b}{\sqrt{a^2+b^2}} \leq \cos\theta, \end{cases} \tag{C11}$$

where θ is the angle between the beam axis and detector, a and b are height and length of the detector, respectively. The probability of the event detected at the detector is averaged over the angle within the detector.

4. σ_μ dependence

g for a finite σ_μ, which corresponds to μ^- DAR forming a bound state, is

$$\begin{aligned} g(\omega_\nu, T; \tau_\mu) = &\int_{-T}^{0} dt_- \int_{-\frac{1}{2}t_-}^{T+\frac{1}{2}t_-} dt_+ \frac{|\vec{v}_{\nu_e}| t_- \sin(\omega_{\nu_e} t_-)}{\vec{v}_{\nu_e}^2 t_-^2 + 4|\vec{p}_{\nu_e}|^2 \sigma_{\nu_e}^2} e^{-\frac{(\vec{v}_\mu - \vec{v}_{\nu_e})^2}{\sigma_\mu + \sigma_{\nu_e}} \left(t_+ - \tilde{T}_L\right)^2} e^{-\frac{2t_+}{\tau_\mu}} \\ &+ \int_{0}^{T} dt_- \int_{\frac{1}{2}t_-}^{T-\frac{1}{2}t_-} dt_+ \frac{|\vec{v}_{\nu_e}| t_- \sin(\omega_{\nu_e} t_-)}{\vec{v}_{\nu_e}^2 t_-^2 + 4|\vec{p}_{\nu_e}|^2 \sigma_{\nu_e}^2} e^{-\frac{(\vec{v}_\mu - \vec{v}_{\nu_e})^2}{\sigma_\mu + \sigma_{\nu_e}} \left(t_+ - \tilde{T}_L\right)^2} e^{-\frac{2t_+}{\tau_\mu}}, \\ t_+ = \frac{t_1 + t_2}{2}, \; t_- = t_1 - t_2. \end{aligned}$$

For μ^+DAR, μ^+ expands within beam stop and σ_μ is almost the same with T. So σ_μ dependence can be included in T-dependence. For $\mu^\pm$DIF, σ_μ is determined by parent particles' coherence lengths and estimated as 0.1–1 m [4]. It is good to approximate μ as a plane wave for these values.

---

[1] V. Weiskopf and E. Wigner, Z. Phys. **63**, 54 (1930).

[2] M. L. Goldberger and K. M. Watson, Phys. Rev. **136**, 1472 (1964).

[3] K. Ishikawa and Y. Tobita, Prog. Theor. Exp. Phys. **2013**, 073B02 (2013).

[4] K. Ishikawa and Y. Tobita, Ann of Phys, **344**, 118 (2014).

[5] K. Ishikawa and T. Shimomura, Prog. Theor. Phys. **114**, 1201 (2005).

[6] K. A. Olive et. al.,(Particle Data Group), Chi. Phys. **C38**, 090001 (2014).

[7] V. N. Aseev, et. al., Phys. Rev. D **84**, 112003 (2011).

[8] E. Komatsu, et. al., Astrophys. J. Suppl., **192**, 18 (2011).

[9] G. Hinshaw, et. al., arXiv:1212.5226 [astro-ph.CO].

[10] P. A. R. Ade, et. al., arXiv;1303.5076 [astro-ph.CO].

[11] K. Ishikawa and Y. Tobita, Prog. Theor. Phys. **122**, 1111 (2009).

[12] H. Lehman, K. Symanzik, and W. Zimmermann, Nuovo Cim. **1**, 205 (1955).

[13] K. Ishikawa and Y. Tobita, arXiv:1311.6917 [hep-ph].

[14] R. Jost and H. Lehmann, Nuovo Cim. **5**, 1598 (1957).

[15] F. J. Dyson, Phys. Rev. **110**, 1460 (1958).

[16] K. Ishikawa and Y. Tobita, arXiv:1209.5586 [hep-ph].

[17] K. Abazajian, M. Acero, S. Agarwalla, A. Aguilar-Arevalo, C. Albright, et. al., (2012), arXiv:1204.5379 [hep-ph] and references therein.

[18] J. Kopp, P. A. N. Machado, M. Maltoni, and T. Schwetz (2013), JHEP 1305, 050 (2013).

[19] A. A. Aguilar-Arevalo et. al., Phys. Rev. Lett. 110, 161801 (2013).

[20] Chen H, et. al. (MicroBooNE Collab.) Proposal for a New Experiment Using the Booster and NuMI Neutrino Beamlines. FERMILAB-PROPOSAL-0974. Batavia, Ill.: Fermi Natl. Accel. Lab. (2007); Chen H, et. al. (MicroBooNE Collab.) Addendum to Proposal for a New Experiment Using the Booster and NuMI Neutrino Beamlines. Batavia, Ill.: Fermi Natl. Accel. Lab. (2008).

[21] A. Aguilar, et. al., Phys Rev. D **64**, 112007 (2001).

[22] B. Armbruster, et. al., Phys. Rev. D **65**, 112001 (2002).

[23] C. Athanassopoulos et. al. (LSND Collaboration), Phys. Rev. C **58**, 2489 (1998) .

[24] M. Harada, et. al., arXiv:1310.1437 [physics.ins-det].

[25] D. Adey, et. al., arXiv:1308.6822 [physics].

[26] K. Ishikawa, T. Tajima, and Y. Tobita, arXiv:1409.4339[hep-ph].